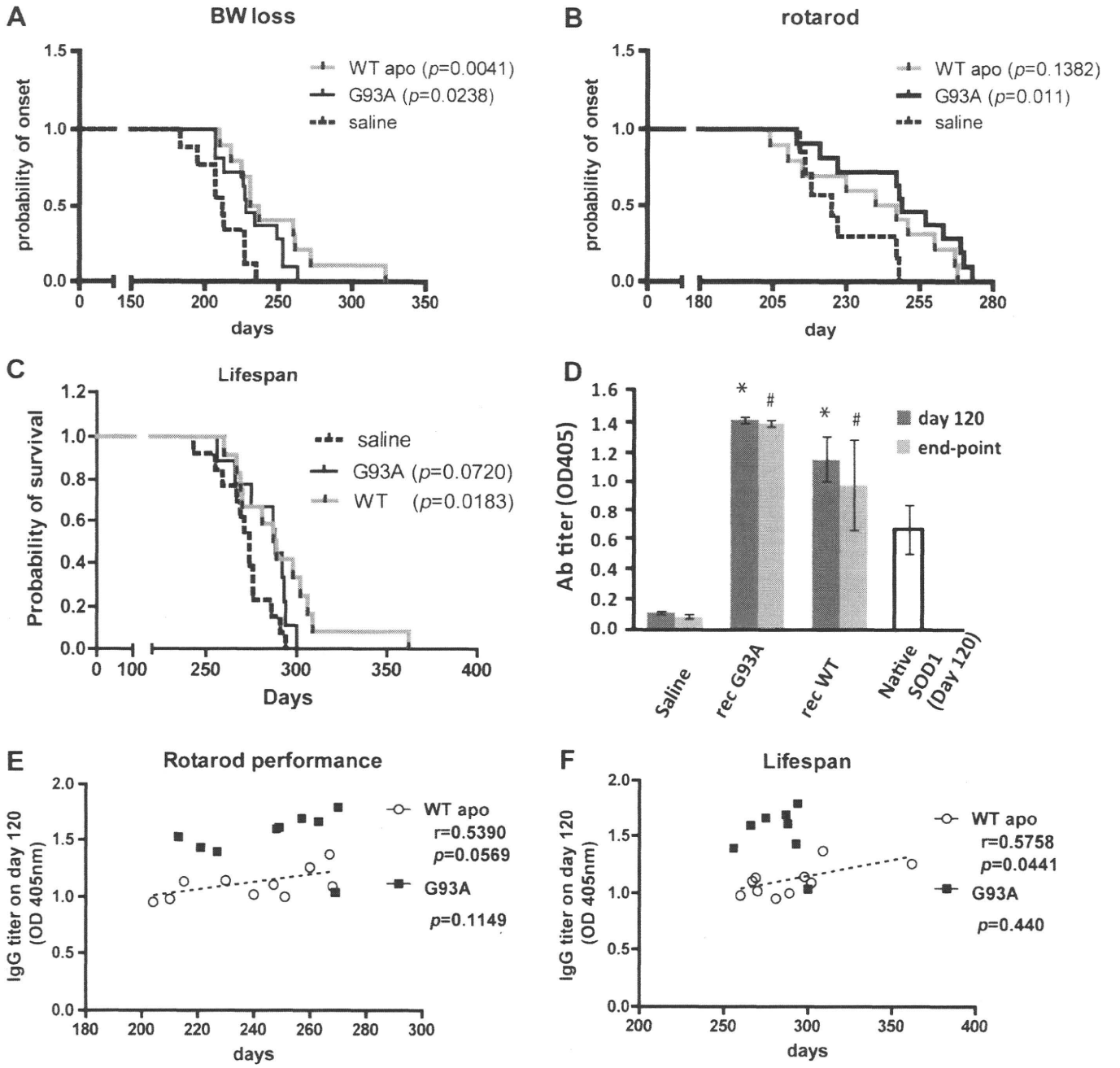

FIGURE 2. Effects of vaccination with recombinant human G93A-apo or wild-type (WT)-apo superoxide dismutase 1 (SOD1) proteins on clinical disease and antibody (Ab) responses in low-copy G93A SOD1 Tg mice (G93AGur^{dl}). **(A, B)** Both the G93A-apo and the WT-apo vaccines significantly delayed the disease onset of G93AGur^{dl} mice. Time of the onset was determined based on body weight (BW) loss **(A)** and impaired rotarod performance **(B)**. **(C)** The WT-apo SOD1 vaccine significantly extended the life span of G93AGur^{dl} mice; the G93A-apo SOD1 vaccine showed a nonsignificant trend. $p < 0.05$ by Kaplan-Meyer curve and log-rank test; n = 13 for saline/adjuvant, n = 12 for the WT-apo, n = 9 for G93A vaccinations. **(D)** Ab titers against G93A SOD1 protein. Sera from vaccinated mice (day 120 and end point) were analyzed by ELISA. The WT-apo SOD1 vaccine induced Ab against G93A SOD1 as well as the G93A-apo SOD1 did even at the end point. *$p < 0.01$ versus saline-injected mice at day 120; $^{\#}p < 0.01$ versus saline-injected mice at end point by 1-way analysis of variance with Bonferroni post hoc test. **(E, F)** Correlation analysis between Ab titer and clinical score including rotarod performance **(E)** and life span **(F)**. Antibodies in both the G93A-apo and the WT-apo vaccination were positively correlated with the onset timing of paralysis **(E)**. The WT-apo SOD1 vaccination was positively correlated with longevity ($p = 0.00441$, Spearman $r = 0.6768$); the G93A-apo SOD1 vaccine displayed a lower value for Spearman r (0.0887).

© 2010 American Association of Neuropathologists, Inc.

TABLE. Effect of Vaccinations on Days of Disease Onset and Survival of G93A Mice

Vaccine	Saline	WT-Apo	G93A-Apo		Saline	WT-Apo	G93A-Apo
Median survival	274	288	287.5	Mean survival (d)	272 ± 3.9	291 ± 7.9	283 ± 4.9
Median onset of rotarod impairment	225	243.5	249	Mean onset of Rotarod impairment	228 ± 5.4	239 ± 7.5	249 ± 6.2
Median onset BW loss	212	234	228	Mean onset BW loss	212 ± 6.2	247 ± 10.6	233 ± 5.9
Effect on survival	—	14	13.5	Effect on survival	—	19	11
Effect on rotarod impairment onset	—	18.5	24	Effect on rotarod impairment onset	—	11	21
Effect on onset BW loss	—	22	16	Effect for onset BW	—	35	21

The effect of vaccination with recombinant G93A-apo or the WT-apo SOD1 protein on the delay of the disease onset or extension of the life span of low-copy G93A SOD1 (G93AGur^{dl}) mice. The left columns are median survival or median onset determined by Kaplan-Myer curves. Data in the right columns show the mean days from each vaccination ± SEM (n = 13 for saline, n = 12 for WT, and n = 9 for G93A).

Effect on survival or onset of impaired rotarod performance and body weight (BW) loss were obtained by subtracting the date for saline injection from those for the WT-apo or the G93A-apo SOD1 vaccination. Time of disease onset was determined by BW loss and rotarod performance. All data are days.

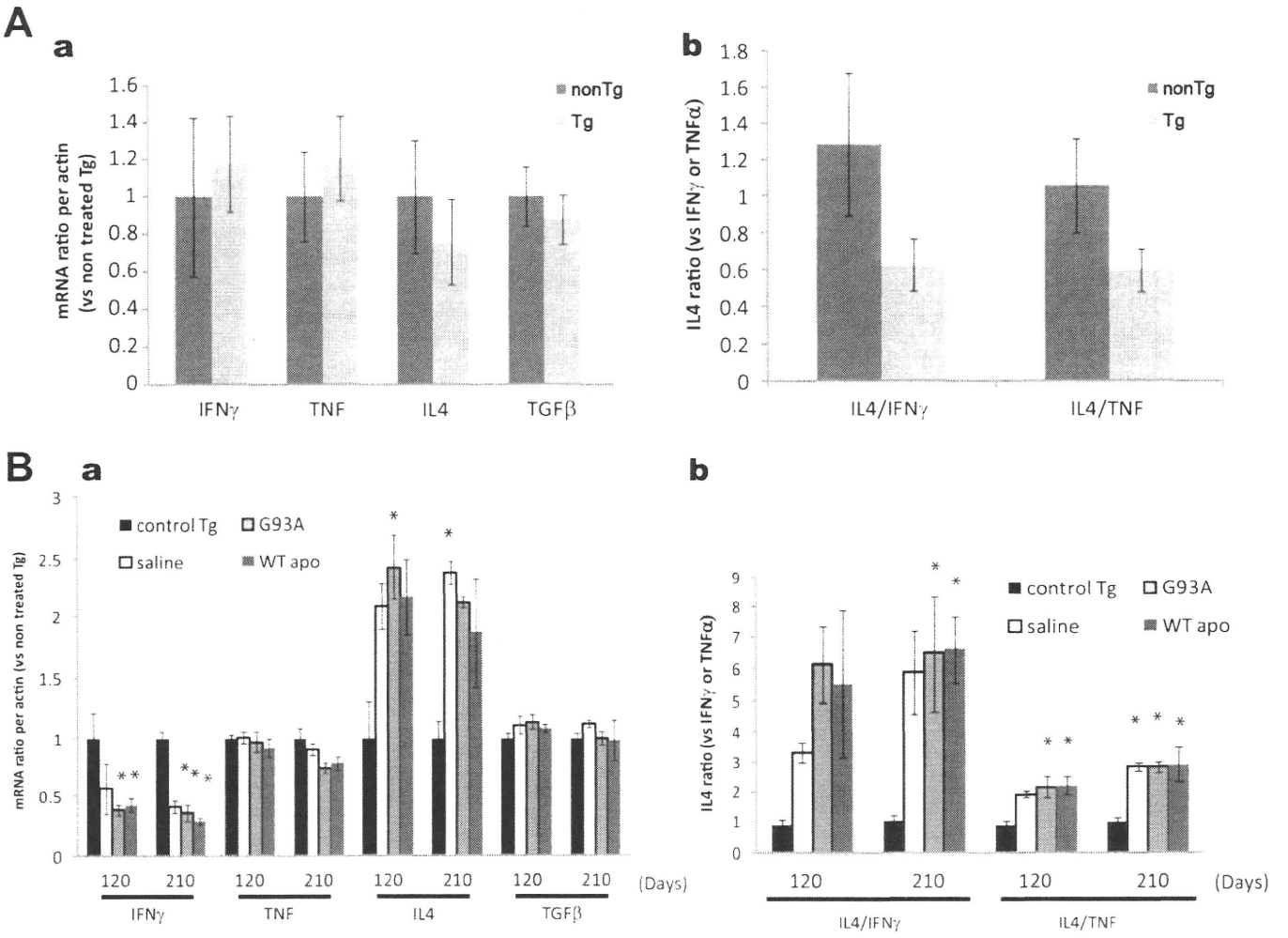

FIGURE 3. Induction of T_H2 deviation in the spinal cord by superoxide dismutase 1 (SOD1) vaccination. **(A, a)** Real-time polymerase chain reaction analysis of mRNA of interferon-γ (IFNγ), tumor necrosis factor (TNF), interleukin-4 (IL-4), and transforming growth factor β (TGFb) in spinal cord tissues from nontransgenic (Tg) wild-type (WT) and nontreated Tg mice at the early presymptomatic stage (day 120). The mean mRNA of each cytokine standardized by actin mRNA is shown. **(A, b)** The ratio of IL-4 to IFNγ or to TNF in each mouse was averaged in each group to estimate the T_H2/T_H1 milieu. The mean IL-4/IFNγ or IL-4/TNF ratio shows a decrease in presymptomatic Tg mice (mean ± SEM, n = 3 for non-Tg mice, and n = 4 for Tg mice). **(B, a)** Real-time polymerase chain reaction analysis of the same cytokines in the spinal cord of the vaccinated mice with WT or G93A SOD1 proteins or saline plus Ribi adjuvant and nontreated Tg controls. **(B, b)** The ratio of IL-4/IFNγ or IL-4/TNF showing that the SOD1 efficiently induced T_H2 protective immunity by inhibiting IFNγ and provoking IL-4. *$p < 0.05$ versus nontreated Tg controls by 1-way analysis of variance with Bonferroni post hoc test (mean ± SEM, n = 3–4 mice).

© 2010 American Association of Neuropathologists, Inc.

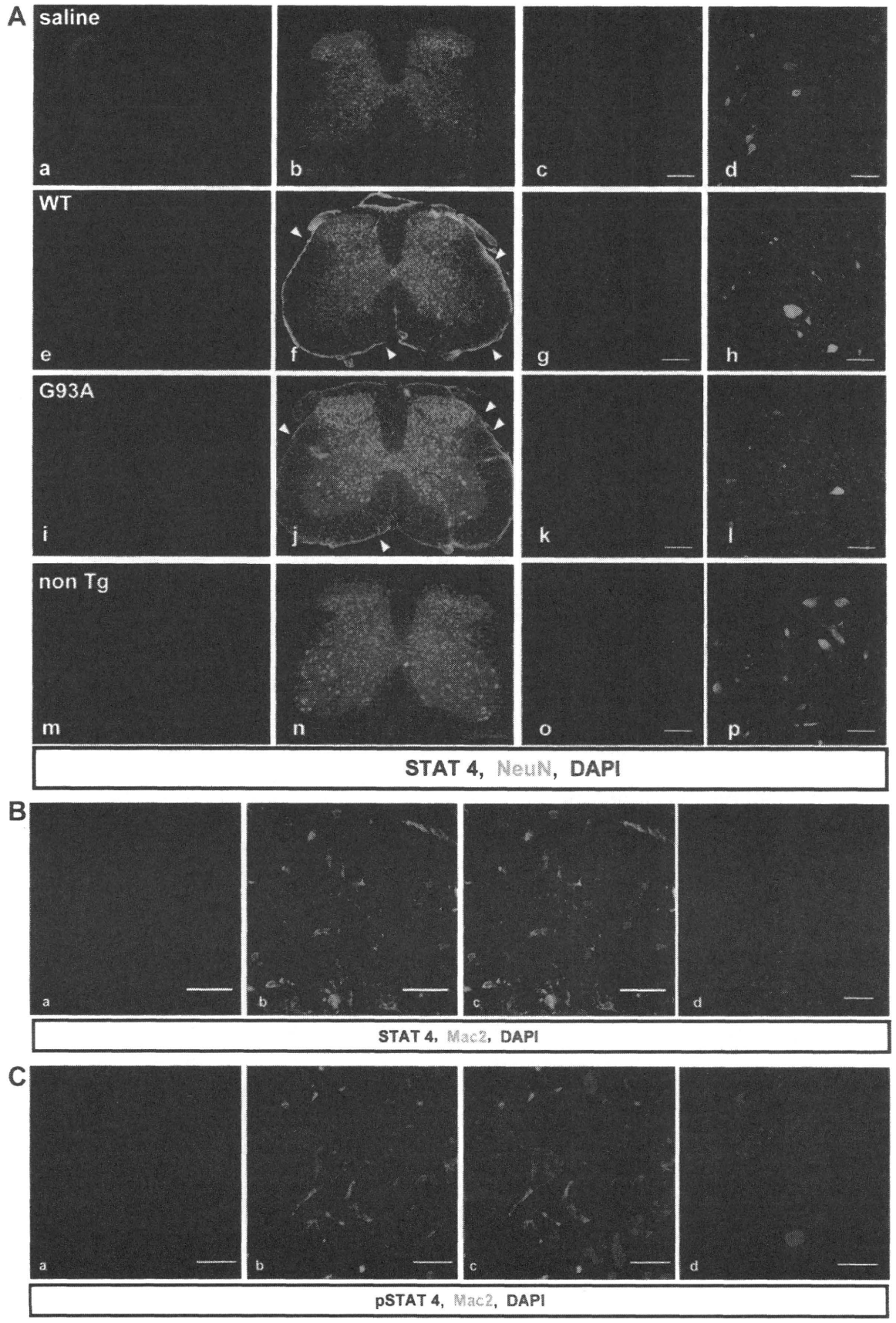

© 2010 American Association of Neuropathologists, Inc.

Enzyme-Linked Immunosorbent Assay

At the ages of 120 days, 210 days, or at the end point, sera were obtained for antibody titration for total IgG, IgG1, IgG2b, and IgG2c against G93A SOD1 protein by enzyme-linked immunosorbent assay (ELISA) as previously described (10), with minor modifications (Methods, Supplemental Digital Content 1, http://links.lww.com/NEN/A178).

Immunofluorescent Analysis

The spinal cords at the level of L4-L5 were resected from 275-day-old mice after perfusion with 4% paraformaldehyde. The sections were incubated in the same fixative for 4 hours and subsequently in PBS containing 20% sucrose and 0.1% sodium azide at 4°C. Cryosections 24 μm thick were incubated with a mixture of primary antibodies and subsequently with a mixture of corresponding secondary antibodies labeled with Alexa 488 or 594 (Invitrogen, Carlsbad, CA). For counterstaining, 4,6-diamidino-2-phenylindole dihydrochloride (Nacalai Tesque) was used. The number of remaining motor neurons in the spinal cord was obtained from averaged count of large NeuN+ cells (<20 μm of the soma) in the anterior horn from 3 samples per mouse. Fluorescent images were obtained using a fluorescent microscope (Keyence, Mississauga, Canada) or a confocal laser microscope equipped with the software EZ-C1 (Nikon, Tokyo, Japan). Antibody information is provided in Methods, Supplemental Digital Content 1, http://links.lww.com/NEN/A178.

Serum Cytokine Quantification

Serum concentrations of TNF, IFNγ, and IL-4 were determined using suspension array system (Bio-Plex Pro Mouse Cytokine; BioRad, Hercules, CA) according to the manufacturer's protocol (Methods, Supplemental Digital Content 1, http://links.lww.com/NEN/A178).

Cytokine Profiling in the Spleen and the Spinal Cord by Real-Time Polymerase Chain Reaction

Cytokines and transcription factors including IFNγ, TNF, transforming growth factor β1 (TGFβ), IL-4, forkhead box P3, and RAR-related orphan receptor γ were investigated for their messenger RNA (mRNA) expression level by real-time polymerase chain reaction (PCR) system, as described with minor modifications (26). On days 120 and 210, total RNA was purified using TRIzol and RNA purification kit (Invitrogen), and an equal amount of total RNA was reacted with reverse transcriptase (Superscript III; Invitrogen) to generate complementary DNA (cDNA). mRNA of cytokines or marker molecules for $CD4^+$ T lymphocytes was analyzed by real-time PCR using the SYBR green system (Roche, Basel, Switzerland). The cDNA level of the target molecules was normalized to that of actin. Detailed procedures including primer sequences are in Methods, Supplemental Digital Content 1, http://links.lww.com/NEN/A178.

Statistics

The survival and clinical onset data were analyzed by Kaplan-Meyer curve and log-rank tests. The effect of a single factor on the difference among 3 or more groups was determined by 1-way analysis of variance (ANOVA) with Bonferroni post hoc test. Comparisons between 2 groups were analyzed by unpaired t test. $p < 0.05$ was judged to be significant.

RESULTS

Characterization of Recombinant SOD1s

The purities of recombinant SOD1s were more than 95%, as determined by SDS-PAGE (data not shown). To investigate the precise molecular weight of SOD1 proteins of as-isolated and nonmetallated state (i.e. WT-apo or G93A-apo) versus the holo-state, we performed molecular-size filtration chromatography because it is thought that apo-SOD1s are constantly monomers (27). However, both apo- and holo-SOD1s are dimeric, although the WT-apo sample appeared to contain some monomer form (Fig. 1). Moreover, the elution times of WT-apo and G93-apoA were slightly faster than those of the holo-types, which could reflect looser structures of apo-SOD1s.

Vaccination With Recombinant WT-Apo SOD1 Extends the Life Expectancy and Delays Disease Onset

$G93AGur^{dl}$ mice were immunized with recombinant G93A-apo SOD1 or WT-apo SOD1 using Ribi adjuvant. Recombinant WT-apo SOD1 was used because of its broader applications regardless of mutation types in SOD1 gene and because, like mutant SOD1, it is misfolded (22). The G93A-apo vaccine significantly delayed the onset of paralysis assessed by BW change and rotarod performance tests (Figs. 2A, B). The WT-apo SOD1 vaccination also significantly suppressed BW loss and showed a trend to preserving the rotarod performance, although this was not significant. The difference of onset time was 18 or 22 days in the WT-apo- and 24 or 16 days in the G93A-apo vaccinated mice, as assessed rotarod tests or BW change, respectively (Table). In addition, both vaccines prolonged the life spans compared with saline/adjuvant–injected controls by 14 and 13.5 days for WT-apo and G93A-apo vaccine, respectively. The log-rank test determined statistical significance only for the WT-apo SOD1 vaccinations ($p = 0.0183$ for the WT-apo; $p = 0.0720$ for the G93A-apo). Notably, the mean life span

FIGURE 4. Signal transducers and activators of transcription 4 (STAT4), a transcription factor for interferon-γ (IFNγ), is abundantly expressed in active microglia of G93A transgenic (Tg) mice. **(A)** Double immunostaining for STAT4 (red) and NeuN (green) in the spinal cord of vaccinated 275-day-old mice. The left 2 columns **(a, b, e, f, i, j, m, n)** and the right 2 columns **(c, d, g, h, k, l, o, p)** are images obtained from the fluorescent microscope and confocal laser microscope, respectively. Expression of STAT4 does not merge with NeuN. Scale bar = 50 μm. **(B, C)** Confocal micrographs of double immunofluorescent analysis for STAT and Mac2 or phosphorylated STAT4 and Mac2 in the spinal cord of $G93AGur^{dl}$ mice. **(a–c)** Saline/adjuvant-injected $G93AGur^{dl}$ mice (30 weeks). **(d)** Non-Tg littermate. Scale bar = 30 μm.

© 2010 American Association of Neuropathologists, Inc.

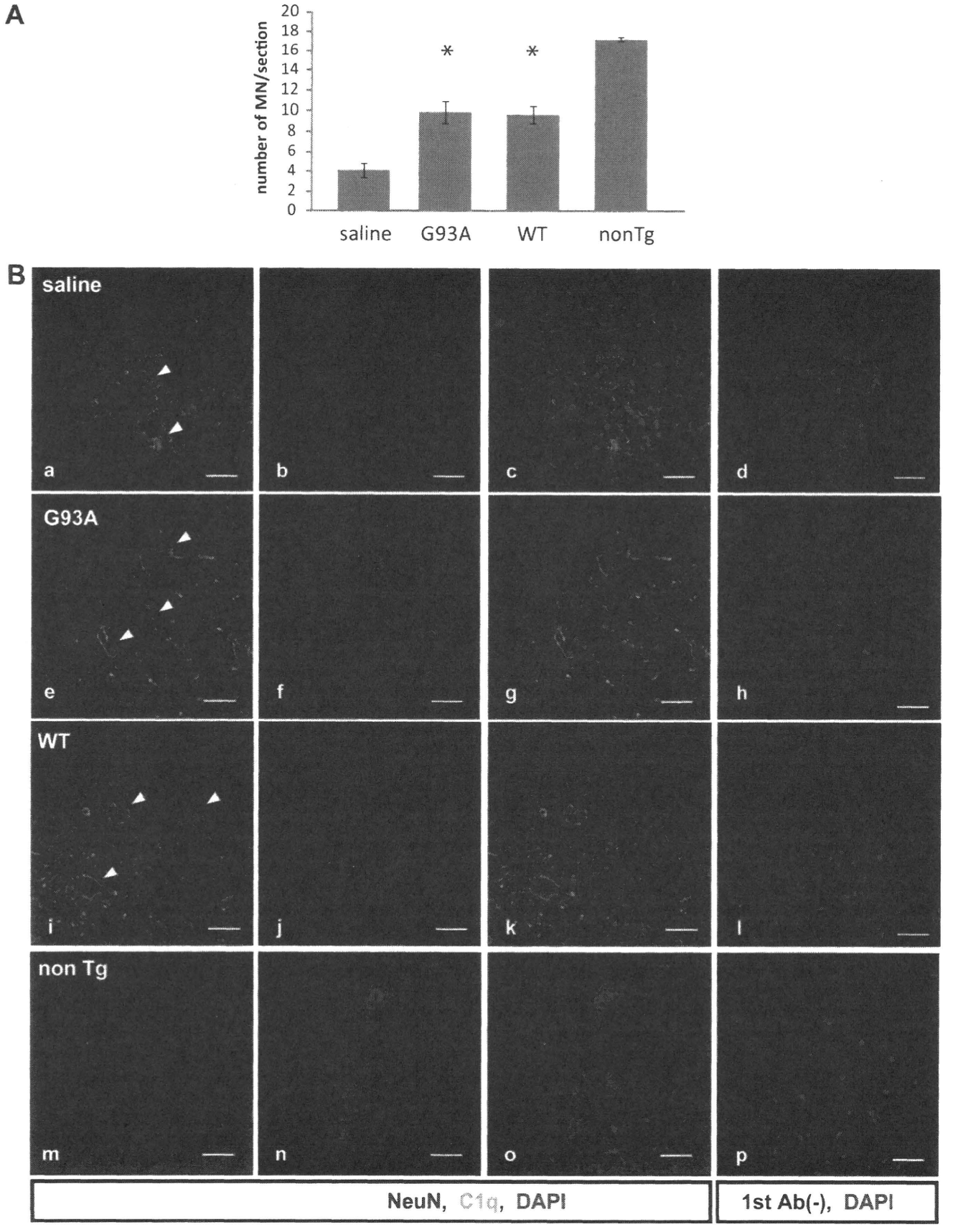

© 2010 American Association of Neuropathologists, Inc.

indicated that there were shorter durations of suffering in G93A-apo–vaccinated mice (Fig. 2C; Table).

We next investigated whether the antibody titer correlated with the therapeutic benefit. The WT-apo and the G93A vaccination induced high titers of anti-G93A SOD1 antibody compared with the native SOD1 vaccination or the saline control (Fig. 2D). The WT-apo vaccine showed a significant positive correlation between the life span and antibody titer ($r = 0.5758$, $p = 0.0041$ by Spearman r) and a trend toward a positive correlation of rotarod testing (Fig. 2E; $r = 0.539$, $p = 0.0569$ by Spearman r). The G93A-apo vaccine showed no significant correlation with either the onset timing (rotarod and BW loss) or survival (Figs. 2E, F). The disease duration was not associated with antibody titer in either the WT-apo or G93A-apo vaccine groups (not shown).

SOD1 Vaccination Potentiates Protective Immunity in the Spinal Cord

mRNA levels of IFNγ, TNF, and IL-4 were determined in the spinal cords of presymptomatic nontreated G93A SOD1 Tg mice (120 days old; n = 3) and non-Tg WT littermates (n = 5). There were slightly higher levels of IFNγ and TNF and lower levels of IL-4 in G93A Tg mice versus non-Tg age-matched mice (Fig. 3Aa). The ratios of IL-4 to IFNγ (IL-4/IFNγ) or TNF (IL-4/TNF), (termed "T_H2/T_H1 ratios") were much lower in the Tg mice (Fig. 3Ab). Comparison between SOD1- or saline plus adjuvant–vaccinated groups and nontreated Tg mice showed a significant reduction of IFNγ in both SOD1 vaccinations versus nontreated G93A Tg controls. Interleukin-4 mRNA was markedly elevated by the SOD1 vaccinations on both days 120 and 210, but only the G93A vaccination on day 120 was statistically significant (by 1-way ANOVA, Bonferroni post hoc test). The saline/adjuvant injection provided an effect comparable to that of the SOD1 vaccination in reducing IFNγ and upregulating IL-4 (Fig. 3Ba). The T_H1/T_H2 milieu is critically influenced by the adjuvant as well as by antigens, and the MPL/TDM adjuvant used has been reported to favor a T_H2 rather than T_H1 milieu (28).

Signal Transducers and Activators of Transcription 4 Induction in Active Microglia in the Spinal Cord

The role of IFNγ in ALS pathogenesis is controversial (14, 29–31). Therefore, we examined the expression pattern of IFNγ in spinal cords of mutant SOD1 Tg mice. Immunohistochemical analysis was performed with an antibody against signal transducers and activators of transcription 4 (STAT4), an activator for transcription of IFNγ under the stimulation of IL-12. There was STAT4 immunoreactivity in the spinal cord of mutant SOD1 Tg mice with or without vaccination (Fig. 4A). Notably, the lamina I in the dorsal horn, which receives nociceptive input, was markedly STAT4+ in both Tg and non-Tg mice (Fig. 4A, a, b, e, f, i, j, m, n). These cells were also NeuN+ (not shown), which might imply a role for IFNγ in pain generation to nociceptive stimulation (32). However, the STAT4+ cells in other areas, including the anterior horn are not costained with anti-NeuN antibody (Fig. 4A, c, d, g, h, k, l, o, p). Therefore, we performed double immunofluorescent staining using antibodies against STAT4 and Mac2. STAT4 was exclusively expressed in Mac2+ active microglia (Fig. 4B). Because phosphorylation is required to activate STAT4 for IFNγ transcription, we examined the presence of phosphorylated STAT4 (pSTAT4) by double immunofluorescent study and found that certain populations of active microglia were pSTAT4+ (Fig. 4C). There was no difference in STAT4 or pSTAT4 levels between vaccinated or nonvaccinated mice (not shown), but the presence of STAT4 in microglia provides evidence that spinal motor neurons are affected by IFNγ from activated microglia. Notably, the fluorescent antimouse IgG antibodies showed meningeal enhancement only in SOD1 vaccinated mice (Fig. 4A, arrowheads), suggesting that vaccine-generated antibodies can reach the spinal cord.

Vaccination With G93A-Apo or WT-Apo SOD1 Attenuates Motor Neuron Loss and Induces Complement C1q Deposition

We next investigated whether the beneficial effect of the vaccination with the G93A-apo or the WT-apo SOD1 correlated with motor neuron protection by counting of NeuN+ remaining anterior horn cells in 275-day-old Tg mice. Both vaccinations with the G93A-apo and the WT-apo significantly attenuated motor neuron loss (Fig. 5A), whereas there was no significant difference in the number of active microglia cells stained by anti–Mac-2 between saline and SOD1 vaccinations was observed (Figure, Supplemental Digital Content 2, http://links.lww.com/NEN/A179).

We then studied the activation of the classic pathway of complement system after vaccination in mice of the same age. C1q, which binds to antigen-antibody complexes at the immunoglobulin Fc domain, is upregulated around motor neurons in SOD1 mutant models before disease onset, suggesting that "danger molecules" are leaked from degenerating motor neurons (33). Double immunofluorescent staining with rat monoclonal anti-C1q and mouse monoclonal anti-NeuN detected C1q around motor neurons in both SOD1-vaccinated and saline-control $G93AGur^{dl}$ mice, but not in age-matched non-Tg littermates. More prominent C1q deposition was detected in SOD1 vaccinated mice than in saline/adjuvant controls (Fig. 5B). These data indicate that the apo-SOD1 vaccination activates the classic pathway in the spinal cord. Because chromogranin interacts with mutant SOD1, promotes

FIGURE 5. Superoxide dismutase 1 (SOD1) vaccination attenuates motor neuron (MN) loss and induces complement deposition around MNs. **(A)** MN count in the spinal cord of vaccinated 275-day-old mice. NeuN+ large anterior horn neurons (>20 μm in size) were counted in 3 slices per mouse; mean numbers per slice are shown. *$p < 0.05$ by 1-way analysis of variance of Bonferroni test (n = 9 for transgenic [Tg], n = 4 for non-Tg; WT = wild-type. **(B)** Induction of complement C1q deposition around MNs by SOD1 vaccination. Confocal micrographs of the spinal cord slices of the vaccinated mice (30 weeks) stained with antibodies against NeuN (red, mouse monoclonal) and C1q (green, rat monoclonal). C1q staining surrounding MNs are indicated with arrowheads; **d, h, l, p** show negative controls in which primary antibodies were eliminated. Scale bar = 30 μm.

© 2010 American Association of Neuropathologists, Inc.

its secretion, and activates microglia (9), the complex formation comprising mutant SOD1–anti-SOD1 antibody-C1q may be facilitated by the SOD1 vaccination.

WT-Apo SOD1 Vaccination Induces a Higher T_H2/T_H1 Milieu Than G93A Vaccination

There were differences in the slowing of the progression in Tg mice between the WT-apo and the G93A SOD1 vaccinations. Because the antibody titer in the G93A-apo vaccination unexpectedly showed no correlation with disease onset or life span as opposed to the WT-apo (Figs. 2E, F), we compared the IgG subclasses induced by the WT-apo and G93A-apo vaccines. Sera of SOD1-vaccinated mice were analyzed on days 120 and 210 by ELISA for IgG1, 2b, and 2c titers. Both the WT-apo and the G93A-apo vaccines induced considerable amounts of each subclass and the G93A vaccination induced more IgG than the WT vaccination. Overall, the difference between the 2 vaccines was statistically significant only on day 120 for IgG1 and day 210 for IgG2b and IgG2c (Fig. 6A, $p < 0.05$ by unpaired t test). The mean ratios of IgG1 to IgG2c (IgG1/IgG2c) (an indicator of the T_H2/T_H1 milieu) were not significantly different between WT and G93A vaccinations on day 120, but on day 210, this ratio was significantly higher in the WT-apo vaccination than in the G93A (Fig. 6Ab, $p < 0.05$ by 1-way ANOVA).

We further measured the quantity of serum cytokines induced by these SOD1 vaccinations using a suspension array system. The antisera from immunized mice with WT or G93A SOD1 vaccine (n = 3/group) on day 120 was analyzed for TNF, IFNγ, and IL-4. The G93A-apo vaccination induced more of the T_H1 cytokines TNF and IFNγ compared with the WT-apo vaccination (Fig. 6B). Interleukin-4 levels were below the detection limit (0.59 pg/mL) in either non-Tg or Tg mice regardless of the type of the vaccination. The analysis of the spleen tissues of the same mice for mRNA quantity of TNF, IFNγ, IL-4, and TGFβ by real-time PCR revealed a clear trend in which IL-4 mRNA in the WT or the G93A vaccination was higher than that in the saline control on day 120. The G93A vaccination tended to induce higher IL-4 than the WT did on day 120. On day 210, IL-4 mRNA remained high in the WT but not in the G93A vaccination sera (Figure, part A, Supplemental Digital Content 2, http://links.lww.com/NEN/A179). No significant differences in expression levels of forkhead box P3 or RAR-related orphan receptor γt, a marker for regulatory T-cell or a T_H1 7 cells, respectively, between control and vaccinated groups were observed (data not shown).

We then analyzed the relationship between IgG subclass and the therapeutic effect of the vaccinations. In the WT-apo vaccination there was a positive correlation between IgG2b titer and the date of the onset (Figure, part B, Supplemental Digital Content 3, http://links.lww.com/NEN/A180, b;

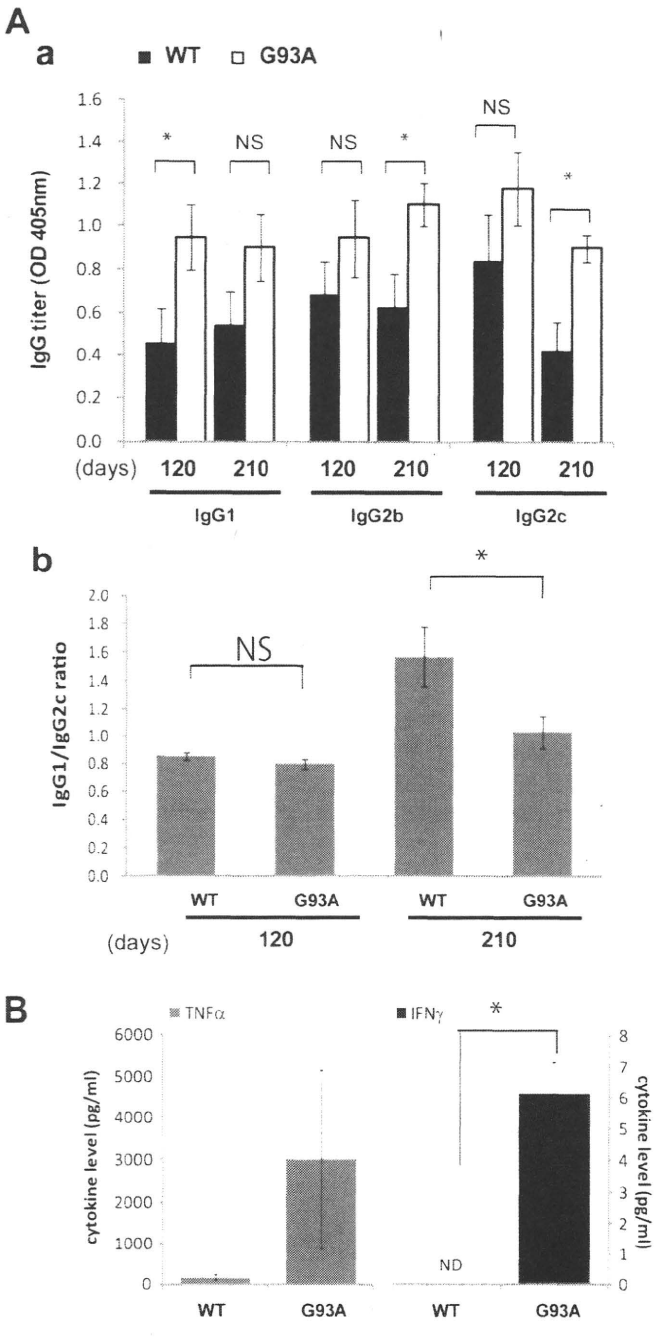

FIGURE 6. Analysis of sera for acquired immunity by superoxide dismutase 1 (SOD1) vaccination. **(A, a)** ELISA for IgG subclasses induced by the SOD1 vaccination. The titer for IgG1, 2b, and 2c against the G93A-apo SOD1 was obtained from sera of wild-type (WT) and G93A SOD1-vaccinated mice at day 120 and 210 and expressed as optical density (OD) 405 nm (mean ± SEM; each group, n = 4 or 5). *$p < 0.05$, NS indicates not significant by unpaired t test. **(A, b)** The ratio of IgG1 to IgG2c (IgG1/IgG2c) was obtained in each mouse and the data averaged (mean ± SEM for each group, n = 4 or 5). *$p < 0.05$ by 1-way analysis of variance with Bonferroni post hoc test. **(B)** Serum cytokine concentrations. Sera from WT or G93A SOD1 vaccination (n = 3) were analyzed for the quantification of interferon gamma (IFNγ) and tumor necrosis factor (TNF) using a suspension array system. Each bar shows the mean concentration from 3 mice ± SEM. *$p < 0.05$ by unpaired t test. ND indicates not detected (under the lowest value of standard curve (0.17 pg/mL).

© 2010 American Association of Neuropathologists, Inc.

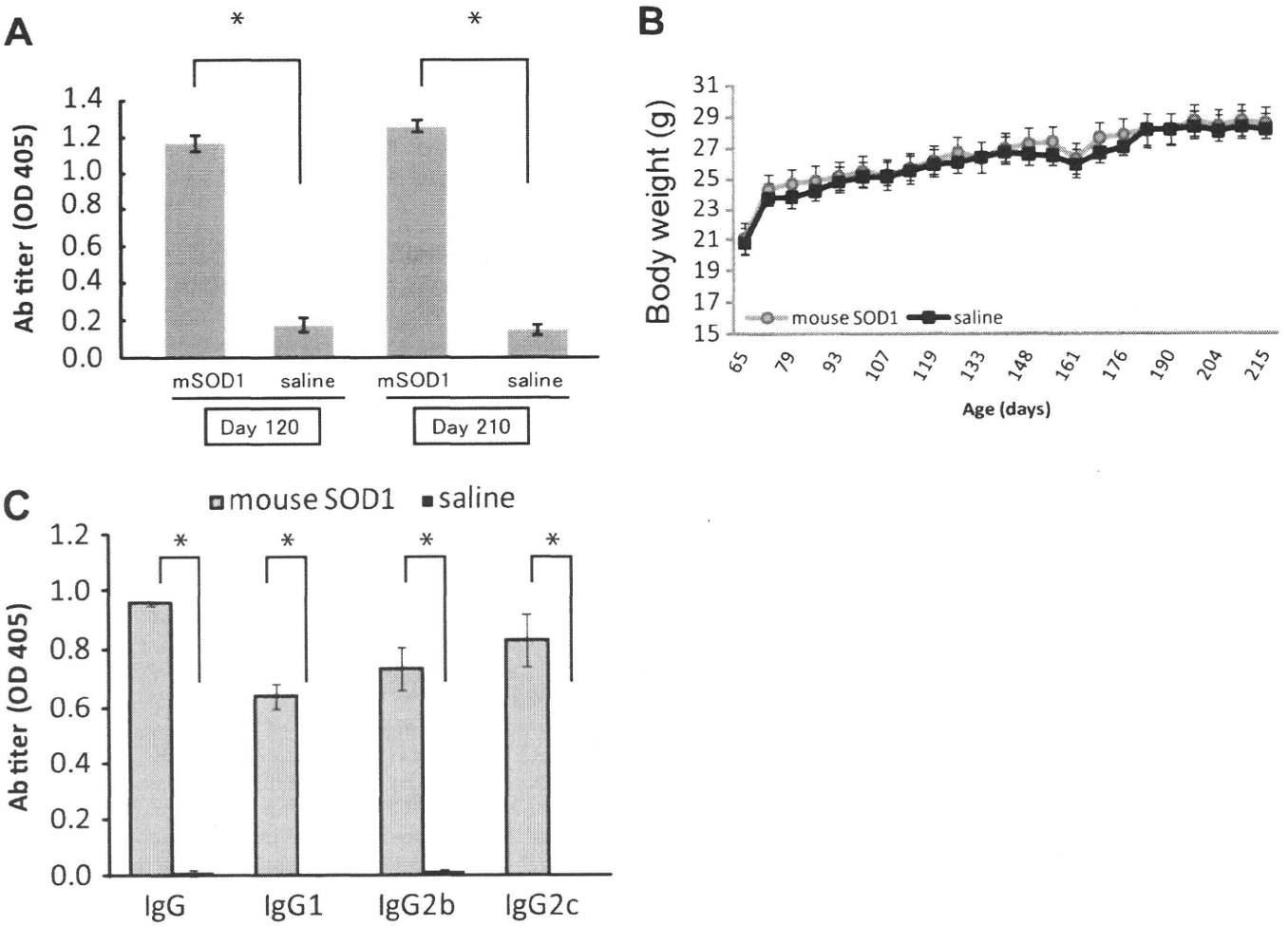

FIGURE 7. Vaccination of nontransgenic (non-Tg) mice using recombinant wild-type (WT) superoxide dismutase 1 (SOD1) protein effectively induces antibody with no detectable detrimental effect. **(A)** ELISA of sera of non-Tg mice vaccinated with mouse SOD1 and saline with adjuvant at days 120 and 210 (n = 5 in each group). Data show mean ± SEM (n = 5). *$p < 0.01$ by 1-way analysis of variance of Bonferroni test. **(B)** Comparison of body weights after vaccination between mouse SOD1-vaccinated and saline/adjuvant–injected controls. Each point shows mean body weight (g) of 5 mice per group. **(C)** ELISA for IgG subclasses induced by mouse SOD1 vaccination. The titer for IgG1, 2b, and 2c against recombinant mouse SOD1 was determined in sera from SOD1-vaccinated and control saline/adjuvant–injected mice at day 210 and expressed as OD 405 nm (mean ± SE forSE for each group, n = 5). *$p < 0.01$ by 1-way analysis of variance of Bonferroni test.

$r = 0.7333$, $p = 0.0156$, by Spearman r), whereas IgG1 and IgG2c showed no significant correlation (Figure, part B, a, c, Supplemental Digital Content 3, http://links.lww.com/NEN/A180). By contrast, there was no positive correlation of the G93A vaccination with any IgG subtype. Rather, the IgG1 titer was negatively correlated to the survival effect (Figure, part B, d, Supplemental Digital Content 3, http://links.lww.com/NEN/A180; $r = -0.5879$, $p = 0.0403$, by Spearman r).

Antibody Induction in Non-Tg Mice by Vaccination With Murine WT SOD1

Because the human WT SOD1 is a foreign antigen to mice, antibody is generally easily induced. For human trials, induction of the antibody against human WT-SOD1 in human body would be required. Therefore, we investigated whether the murine WT-apo SOD1 induced antibody by breaking immunologic tolerance to endogenous SOD1 in mice. Vaccination of non-Tg C57BL/6 mice with recombinant mouse WT-apo SOD1 induced antibody against mouse SOD1 at days 120 and 210 (Fig. 7A). Simultaneously, the adverse reactions of the vaccination were monitored for BW loss (Fig. 7B), movement, hair length, spontaneous activity, and provoked biting as well as observation of tissue hemorrhage or anemia at autopsy. These analyses displayed no abnormalities that could be attributed to vaccination. The analysis of IgG subclass profile showed that all the subclasses including IgG1, IgG2b, and IgG 2c were comparably elevated (Fig. 7C), indicating that both T_H1 and T_H2 immunity is induced in non-Tg mice.

DISCUSSION

In this report, we demonstrate a beneficial effect of vaccination with the WT-apo SOD1 protein to prolong the life

© 2010 American Association of Neuropathologists, Inc.

span of G93A SOD1 Tg mice. The chief effect was delaying the disease onset rather than slowing its progression. The G93A SOD1 vaccine also delayed the onset significantly and showed a trend to prolonging the life span. This result is in agreement with our previous finding that the vaccination with the G93A-apo SOD1 protein against G37R SOD1 mice (5 times higher) led to a 3-week delay of onset and a 4-week prolongation of life span, whereas the same vaccination of high-copy G93A SOD1 (G93AGur) mice (17 times higher) was not effective (10). Therefore, the expression level of the mutant protein in the Tg mice may determine the vaccine effect, particularly in the late stage. Because there generally are 1 or 2 copies of the mutant SOD1 gene in ALS patients, our results indicate that further development of vaccination aiming not only for prevention but also for disease inhibition after onset is warranted.

Unexpectedly, the apo-form of the SOD1 was a dimer, although the precise molecular features of the WT-apo SOD1 are unclear. The apo-SOD1 of both WT and G93A are slightly larger molecules than the holo-SOD1s, indicating that the apo-form of SOD1s form nonnative dimers. Intriguingly, the previous report showed that a nonnative SOD1 dimer is a common finding in mutant and sporadic ALS (24). Therefore, the misfolded dimeric conformation might mediate the vaccine effect of the WT-apo SOD1. Because of its utility regardless of the mutation type, the protective effect of the WT-apo SOD1 in $G93AGur^{dl}$ mice may represent a widely applicable paradigm. We observed no detrimental effect of WT-apo SOD1 vaccination in G37R Tg mice, but there seemed to be some beneficial effect (personal observation). We and others have reported potential misfolding property of the WT SOD1 when posttranslationally modified such as monomerization (21) or oxidation (34), which may account for the effect of the WT-apo SOD1 vaccination. Therefore, further modification by narrowing the critical domains for misfolding or by specifying more aberrant structures such as oligomer or aggregates is a potential strategy for developing vaccines against mutant SOD1-linked ALS.

The precise mechanisms of the beneficial effects of vaccination with the misfolded SOD1 protein are unclear. We found that C1q increased around the remaining motor neurons and that IgG immunoreactivity increased in the spinal cord meninges. Moreover, the blood-brain barrier of mutant SOD1 Tg mice is fragile (35), and recent studies show $CD4^+$ T-cell proliferation in the spinal cord of mutant SOD1 Tg mice (17, 18). Therefore, it is conceivable that immune-related molecules or cells may easily penetrate into the CNS in mutant SOD1-linked ALS patients and that vaccine-induced antibodies could directly target extracellular SOD1 in the spinal cord. Although immunohistochemistry showed no obvious change in the SOD1 aggregates by the vaccination (not shown), this indicates that only small fractions of soluble misfolded species might participate in the extracellular toxicity.

Our results indicate that there is induction of protective immunity by vaccination with the Ribi adjuvant. The effect of both SOD1 vaccinations on T_H2 deviation in the spinal cord is striking. Moreover, STAT4 analysis suggests that activated microglia in the spinal cord of mutant SOD1 Tg mice are the source of IFNγ. Indeed, a recent report also showed that STAT4 is chiefly expressed in the active microglia in the cerebral white matter in multiple sclerosis (36). Active microglia expressing Mac-2 in the spinal cords are detected in presymptomatic mutant SOD1 Tg mice but not in non-Tg or WT SOD1 Tg mice (personal observation). Thus, microglia-derived IFNγ might be a pathogenic proinflammatory factor in mutant SOD1-linked ALS. Indeed, accumulating evidence also indicates the detrimental effect of IFNγ in the CNS, including oxidative stress (14), mitochondrial damage (30), and MHC class II+ cell proliferation (18). On the other hand, it should be noted that the toxicity of IFNγ is context-dependent and that it is regulated by a complex crosstalk between microglia and T-cell subtypes (37). It was reported that the stimulation of microglial cells with IFNγ rescues cells with various toxic challenges through the induction of IGF-1 (38) or IGF-2 (39). A recent study also shows that a low dose of IFNγ provides neuroprotection by enhancing neurogenesis in the amyloid precursor protein Tg mice (40). Therefore, the effects of IFNγ in the CNS are complex, and synergistic effects of other proinflammatory cytokines (e.g. TNF) in specific conditions likely are involved. Interestingly, the saline/adjuvant injection also promoted T_H2 deviation, possibly as a result of using the Ribi adjuvant (29). This result indicates that the adjuvant is crucial to acquire desirable effect of the vaccination, especially in ALS mutant mice. However, because of the lack of a therapeutic effect of saline/adjuvant injection, T_H2 deviation is not the primary mediator of the beneficial effects of vaccination.

We previously reported that late-stage G37R Tg mice with SOD1 vaccination had greater Mac2+ microglia than control mice (10). However, in the present study, analysis of the mice at the same point showed no significant difference in the number of Mac2+ microglia. Therefore, it may be that longer-lived mice with SOD1 vaccination showed more abundant microgliosis. Further analyses including in situ hybridization are needed to clarify this issue because of the diverse and complicated functions of microglia.

We show here that the both SOD1 vaccinations increased IL-4 mRNA levels in the spleen at an early time point and that there was a significant difference in IgG2c titer and IgG1/IgG2c ratio between the WT-apo and the G93A-apo vaccinations at the late stage. These results suggest that peripheral IL-4 may drive a T_H2 milieu from the early presymptomatic stage in the spinal cord, and circulating IFNγ may have some detrimental effect in the later period. Thus, the amount of IFNγ or TNF in the serum at the preclinical stage might be a useful marker for selecting an appropriate vaccine and adjuvant. Furthermore, the titer of each IgG subclass was not positively correlated in G93A-apo vaccination; rather, IgG1 titer was negatively correlated to the life span (Figure, Supplemental Digital Content, part B, d, http://links.lww.com/NEN/A180). These results suggest that T_H1/T_H2 regulation is unbalanced by the G93A vaccination in the Tg mice with the same mutation. Taken together, T_H1 deviation in the G93A vaccination in the later stage might counteract the effect to slow the progression. A recent report shows that IFNγ is increased in the serum of ALS patients (41). Moreover, systemically injected IFNγ distributes in the

© 2010 American Association of Neuropathologists, Inc.

brain (42) and it is known to disturb the immunologic privilege by the induction of MHC class I antigen in CNS cells (43). On the other hand, ablation of $CD4^+$ cells in mutant SOD1 Tg mice accelerated the ALS phenotype, which is mediated by microglial inhibition of IGF-1 (17). It was also reported that intravenous injection of regulatory or effecter T-cells significantly prolongs the longevity of G93A Tg mice (19). In a spinal cord injury model, externally injected macrophages potentiated the repair of damaged tissue by halting microglial activation (44). In such cases, anti-inflammatory cytokines including IL-4 (17) and IL-10 (45) mediate transfer of protective signals to microglia. Because there is potentially aberrant immunity in ALS, vaccinations should be cautiously designed. Considering recent conflicting reports as for therapeutic outcomes of a glatiramer acetate vaccination (46–49), in which an adjuvant is used only in the successful case (49) but not in other failures (46–48), it is possible that the repetitive challenges of a neuroprotective antigen without adjuvant may not suffice to evoke protective immunity. Therefore, in light of current understanding of the role of the inflammation in neurodegeneration, T_H1 /T_H2 balance may determine a detrimental/protective direction of neurons by regulating microglial function (50). Thus, it is important to recognize that a proper combination of antigen and adjuvant may synergistically augment the therapeutic effect of vaccination. Notably, the positive correlation between IgG2b (a subclass induced by TGFβ) and the therapeutic effect, including delay of disease onset and prolongation of the life span, prompts us to consider the benefit of mucosal immunity such as nasal or intestinal vaccination in which neuroprotective cytokines such as TGFβ and IL-4 are induced (51).

Vaccination of non-Tg mice with mouse WT SOD1 effectively induced antibody but did no overt harm. This is very important for the future application of anti-SOD1 antibody in terms of potential adverse reactions and immunologic tolerance. Abundant IgG2c as well as IgG1 was induced by the vaccination indicating that T_H1 immunity is provoked. Therefore, further modifications for the improvement of the vaccine effect include the development of misfolding structure–targeted vaccines, such as an oligomer or more narrowed sequences involved in the pathogenesis, the choice of adjuvant, and the route of vaccination.

In conclusion, our results indicate that WT-apo SOD1 may be a candidate as a vaccine for familial ALS patients with SOD1 mutations. Moreover, they suggest that induction of protective immunity and immunomodulation to suppress T_H1 immunity, particularly at the later stage, may enhance the outcome. Despite the advantage of passive immunization, which can abolish such immune response considerably, further improvement of vaccines will prove beneficial to familial ALS patients because of their long-lasting effects and of potential noninvasive ways for overcoming adverse reactions.

ACKNOWLEDGMENTS

The authors thank H. Kita and S. Nakamura for the technical assistance. The authors also thank Central Research Laboratory of Shiga University of Medical Science for experimental support. The authors are grateful to Ube Industries Ltd for kindly providing the recombinant human SOD1, chemically modified with 2-mercaptoethanol (2-ME-SOD1).

REFERENCES

1. Dion PA, Daoud H, Rouleau GA. Genetics of motor neuron disorders: New insights into pathogenic mechanisms. Nat Rev Genet 2009;10:769–82
2. Rosen DR, Siddique T, Patterson D, et al. Mutations in Cu/Zn superoxide dismutase gene are associated with familial amyotrophic lateral sclerosis. Nature 1993;362:59–62
3. Gurney ME, Pu H, Chiu AY, et al. Motor neuron degeneration in mice that express a human Cu,Zn superoxide dismutase mutation. Science 1994;264:1772–75
4. Clement AM, Nguyen MD, Roberts EA, et al. Wild-type nonneuronal cells extend survival of SOD1 mutant motor neurons in ALS mice. Science 2003;302:113–17
5. Lobsiger CS, Cleveland DW. Glial cells as intrinsic components of non–cell-autonomous neurodegenerative disease. Nat Neurosci 2003;10:1355–60
6. Ilieva H, Polymenidou M, Cleveland DW. Non–cell autonomous toxicity in neurodegenerative disorders: ALS and beyond. J Cell Biol 2009;187:761–72
7. Aguzzi A, Rajendran L. The transcellular spread of cytosolic amyloids, prions, and prionoids. Neuron 2009;64:783–90
8. Frost B, Diamond MI. Prion-like mechanisms in neurodegenerative diseases. Nat Rev Neurosci 2010;11:155–59
9. Urushitani M, Sik A, Sakurai T, et al. Chromogranin-mediated secretion of mutant superoxide dismutase proteins linked to amyotrophic lateral sclerosis. Nat Neurosci 2006;9:108–18
10. Urushitani M, Ezzi SA, Julien JP. Therapeutic effects of immunization with mutant superoxide dismutase in mice models of amyotrophic lateral sclerosis. Proc Natl Acad Sci U S A 2007;104:2495–500
11. Cao C, Lin X, Wahi MM, et al. Successful adjuvant-free vaccination of BALB/c mice with mutated amyloid beta peptides. BMC Neurosci 2008;9:25
12. Kutzler MA, Cao C, Bai Y, et al. Mapping of immune responses following wild-type and mutant Abeta42 plasmid or peptide vaccination in different mouse haplotypes and HLA class II Tg mice. Vaccine 2006;24:4630–39
13. He BP, Wen W, Strong MJ. Activated microglia (BV-2) facilitation of TNF-alpha–mediated motor neuron death in vitro. J Neuroimmunol 2002;128:31–38
14. Mir M, Asensio VJ, Tolosa L, et al. Tumor necrosis factor alpha and interferon gamma cooperatively induce oxidative stress and motoneuron death in rat spinal cord embryonic explants. Neuroscience 2009;162:959–71
15. Zhao W, Xie W, Xiao Q, et al. Protective effects of an anti-inflammatory cytokine, interleukin-4, on motoneuron toxicity induced by activated microglia. J Neurochem 2006;99:1176–87
16. Kawamata T, Akiyama H, Yamada T, et al. Immunologic reactions in amyotrophic lateral sclerosis brain and spinal cord tissue. Am J Pathol 1992;140:691–707
17. Beers DR, Henkel JS, Zhao W, et al. $CD4^+$ T cells support glial neuroprotection, slow disease progression, and modify glial morphology in an animal model of inherited ALS. Proc Natl Acad Sci U S A 2008;105:15558–63
18. Chiu IM, Chen A, Zheng Y, et al. T lymphocytes potentiate endogenous neuroprotective inflammation in a mouse model of ALS. Proc Natl Acad Sci U S A 2008;105:17913–18
19. Banerjee R, Mosley RL, Reynolds AD, et al. Adaptive immune neuroprotection in G93A-SOD1 amyotrophic lateral sclerosis mice. PLoS One 2008;3:e2740
20. Rakhit R, Robertson J, Vande Velde C, et al. An immunological epitope selective for pathological monomer–misfolded SOD1 in ALS. Nat Med 2007;13:754–59
21. Furukawa Y, O'Halloran TV. Amyotrophic lateral sclerosis mutations have the greatest destabilizing effect on the apo- and reduced form of SOD1, leading to unfolding and oxidative aggregation. J Biol Chem 2004;279:17266–74

© 2010 American Association of Neuropathologists, Inc.

22. Urushitani M, Kurisu J, Tateno M, et al. CHIP promotes proteasomal degradation of familial ALS-linked mutant SOD1 by ubiquitinating Hsp/Hsc70. J Neurochem 2004;90:231–44
23. Shibata N, Hirano A, Kobayashi M, et al. Presence of Cu/Zn superoxide dismutase (SOD) immunoreactivity in neuronal hyaline inclusions in spinal cords from mice carrying a transgene for Gly93Ala mutant human Cu/Zn SOD. Acta Neuropathol 1998;95:136–42
24. Gruzman A, Wood WL, Alpert E, et al. Common molecular signature in SOD1 for both sporadic and familial amyotrophic lateral sclerosis. Proc Natl Acad Sci U S A 2007;104:12524–29
25. Fujiwara N, Nakano M, Kato S, et al. Oxidative modification to cysteine sulfonic acid of Cys111 in human copper-zinc superoxide dismutase. J Biol Chem 2007;282:35933–44
26. Sato T, Takeuchi S, Saito A, et al. Axonal ligation induces transient redistribution of TDP-43 in brainstem motor neurons. Neuroscience 2009;164:1565–78
27. Tiwari A, Liba A, Sohn SH, et al. Metal deficiency increases aberrant hydrophobicity of mutant superoxide dismutases that cause amyotrophic lateral sclerosis. J Biol Chem 2009;284:27746–58
28. Baldridge JR, Yorgensen Y, Ward JR, et al. Monophosphoryl lipid A enhances mucosal and systemic immunity to vaccine antigens following intranasal administration. Vaccine 2000;18:2416–25
29. Ferri A, Nencini M, Cozzolino M, et al. Inflammatory cytokines increase mitochondrial damage in motoneuronal cells expressing mutant SOD1. Neurobiol Dis 2008;32:454–60
30. Ford L, Rowe D. Interleukin-12 and interferon-gamma are not detectable in the cerebrospinal fluid of patients with amyotrophic lateral sclerosis. Amyotroph Lateral Scler Other Motor Neuron Disord 2004;5:118–20
31. Rivest S. Regulation of innate immune responses in the brain. Nat Rev Immunol 2009;9:429–39
32. Racz I, Nadal X, Alferink J, et al. Interferon-gamma is a critical modulator of CB(2) cannabinoid receptor signaling during neuropathic pain. J Neurosci 2008;28:12136–45
33. Lobsiger CS, Boillee S, Cleveland DW. Toxicity from different SOD1 mutants dysregulates the complement system and the neuronal regenerative response in ALS motor neurons. Proc Natl Acad Sci U S A 2007; 104:7319–26
34. Ezzi SA, Urushitani M, Julien JP. Wild-type superoxide dismutase acquires binding and toxic properties of ALS-linked mutant forms through oxidation. J Neurochem 2007;102:170–78
35. Zhong Z, Deane R, Ali Z, et al. ALS-causing SOD1 mutants generate vascular changes prior to motor neuron degeneration. Nat Neurosci 2008; 11:420–22
36. Zeis T, Graumann U, Reynolds R, et al. Normal-appearing white matter in multiple sclerosis is in a subtle balance between inflammation and neuroprotection. Brain 2008;131:288–303
37. Kipnis J, Avidan H, Caspi RR, et al. Dual effect of CD4+CD25+ regulatory T cells in neurodegeneration: A dialogue with microglia. Proc Natl Acad Sci U S A 2004;101:14663–69
38. Gao X, Gillig TA, Ye P, et al. Interferon-gamma protects against cuprizone-induced demyelination. Mol Cell Neurosci 2000;16:338–49
39. Nicholas RS, Stevens S, Wing MG, et al. Microglia-derived IGF-2 prevents TNFα induced death of mature oligodendrocytes in vitro. J Neuroimmunol 2002;124:36–44
40. Baron R, Nemirovsky A, Harpaz I, et al. IFN-gamma enhances neurogenesis in wild-type mice and in a mouse model of Alzheimer's disease. FASEB J 2008;22:2843–52
41. Babu GN, Kumar A, Chandra R, et al. Elevated inflammatory markers in a group of amyotrophic lateral sclerosis patients from northern India. Neurochem Res 2008;33:1145–49
42. Hozumi H, Asanuma M, Miyazaki I, et al. Protective effects of interferon-gamma against methamphetamine-induced neurotoxicity. Toxicol Lett 2008;177:123–29
43. Takeuchi H, Wang J, Kawanokuchi J, et al. Interferon-gamma induces microglial-activation induced cell death: A hypothetical mechanism of relapse and remission in multiple sclerosis. Neurobiol Dis 2006;22:33–39
44. Shechter R, London A, Varol C, et al. Infiltrating blood-derived macrophages are vital cells playing an anti-inflammatory role in recovery from spinal cord injury in mice. PLoS Med 2009;6:e1000113
45. Weiner HL, Lemere CA, Maron R, et al. Nasal administration of amyloid-beta peptide decreases cerebral amyloid burden in a mouse model of Alzheimer's disease. Ann Neurol 2000;48:567–79
46. Haenggeli C, Julien JP, Mosley RL, et al. Therapeutic immunization with a glatiramer acetate derivative does not alter survival in G93A and G37R SOD1 mouse models of familial ALS. Neurobiol Dis 2007;26:146–52
47. Habisch HJ, Schwalenstöcker B, Danzeisen R, et al. Limited effects of glatiramer acetate in the high-copy number hSOD1-G93A mouse model of ALS. Exp Neurol 2007;206:288–95
48. Meininger V, Drory VE, Leigh PN, et al. Glatiramer acetate has no impact on disease progression in ALS at 40 mg/day: A double- blind, randomized, multicentre, placebo-controlled trial. Amyotroph Lateral Scler 2009;10:378–83
49. Angelov DN, Waibel S, Guntinas-Lichius O, et al. Therapeutic vaccine for acute and chronic motor neuron diseases: implications for amyotrophic lateral sclerosis. Proc Natl Acad Sci U S A 2003;100:4790–95
50. Appel SH, Beers DR, Henkel JS. T cell-microglial dialogue in Parkinson's disease and amyotrophic lateral sclerosis: Are we listening? Trends Immunol 2010;31:7–17
51. Bhowmick S, Mazumdar T, Ali N. Vaccination route that induces transforming growth factor beta production fails to elicit protective immunity against *Leishmania donovani* infection. Infect Immun 2009;77: 1514–23

© 2010 American Association of Neuropathologists, Inc.

Hepatocyte growth factor inhibits CNS autoimmunity by inducing tolerogenic dendritic cells and $CD25^+Foxp3^+$ regulatory T cells

Mahdia Benkhoucha[a,b], Marie-Laure Santiago-Raber[a], Gregory Schneiter[a], Michel Chofflon[b], Hiroshi Funakoshi[c], Toshikazu Nakamura[d], and Patrice H. Lalive[a,b,e,1]

[a]Department of Pathology and Immunology, Faculty of Medicine, University of Geneva, 1211 Geneva, Switzerland; [b]Department of Neurosciences, Division of Neurology, and [e]Department of Genetic and Laboratory Medicine, Division of Laboratory Medicine, University Hospital of Geneva, 1211 Geneva, Switzerland; [c]Department of Biochemistry and Molecular Biology, Graduate School of Medicine, and [d]Kringle Pharma Joint Research Division for Regenerative Drug Discovery, Center for Advanced Science and Innovation, Osaka University, 565-0871 Osaka, Japan

Edited* by Michael Sela, Weizmann Institute of Science, Rehovot, Israel, and approved February 22, 2010 (received for review October 28, 2009)

Immune-mediated diseases of the CNS, such as multiple sclerosis and its animal model, experimental autoimmune encephalitis (EAE), are characterized by the activation of antigen-presenting cells and the infiltration of autoreactive lymphocytes within the CNS, leading to demyelination, axonal damage, and neurological deficits. Hepatocyte growth factor (HGF) is a pleiotropic factor known for both neuronal and oligodendrocytic protective properties. Here, we assess the effect of a selective overexpression of HGF by neurons in the CNS of C57BL/6 mice carrying an HGF transgene (HGF-Tg mice). EAE induced either by immunization with myelin oligodendrocyte glycoprotein peptide or by adoptive transfer of T cells was inhibited in HGF-Tg mice. Notably, the level of inflammatory cells infiltrating the CNS decreased, except for $CD25^+Foxp3^+$ regulatory T (T_{reg}) cells, which increased. A strong T-helper cell type 2 cytokine bias was observed: IFN-γ and IL-12p70 decreased in the spinal cord of HGF-Tg mice, whereas IL-4 and IL-10 increased. Antigen-specific response assays showed that HGF is a potent immunomodulatory factor that inhibits dendritic cell (DC) function along with differentiation of IL-10–producing T_{reg} cells, a decrease in IL-17–producing T cells, and down-regulation of surface markers of T-cell activation. These effects were reversed fully when DC were pretreated with anti-cMet (HGF receptor) antibodies. Our results suggest that, by combining both potentially neuroprotective and immunomodulatory effects, HGF is a promising candidate for the development of new treatments for immune-mediated demyelinating diseases associated with neurodegeneration such as multiple sclerosis.

cMet (HGF receptor) | experimental autoimmune encephalitis | immune tolerance | multiple sclerosis | neuroprotection

Hepatocyte growth factor (HGF), also called "scatter factor," is a polypeptide growth factor that belongs to the plasminogen family and consists of a 62-kDa alpha subunit and a 34-kDa beta subunit that form a disulfide-linked heterodimer (1). The molecule was discovered independently as a growth factor in the liver (2, 3) and as a fibroblast-derived effector of epithelial movement and cell–cell interaction (4–6). HGF is a pleiotropic factor that can trigger motility, proliferation, morphogenesis, and organ regeneration in a variety of epithelial cells (7). HGF is able to induce various responses in development (1) and in pathological situations, including tumor progression (8) and suppression of fibrosis (9). The receptor for HGF, cMet, is a tyrosine kinase encoded by the *cMet* proto-oncogene (10, 11). Mice lacking either HGF or its receptor die during embryogenesis, with defects in placenta, liver, and muscle development (12–14).

Both HGF and its receptor cMet are expressed during brain development and persist in the adult (15, 16). cMet is expressed in neurons but also in other brain-resident cells such as oligodendrocytes, astrocytes, and microglia (17–22). HGF promotes axonal outgrowth and regulates the differentiation of various neuronal populations, including sensory, sympathetic, and motor neurons (23, 24). The ability of HGF to promote survival of neurons is as potent as that of several neuroprotective factors, including brain-derived neurotrophic factor, ciliary neurotrophic factor, glial cell line-derived neurotrophic factor, and neurotrophin-3 (23). In addition, HGF is able to induce proliferation and migration of oligodendrocyte precursor cells (OPC) (17, 18, 22) as well as inhibition of the proapoptotic caspase-3 pathway in oligodendrocytes (21). Therefore, HGF could be involved in the processes of neuroprotection, attenuation of oligodendrocyte degeneration, and/or remyelination.

In animal studies, overexpression of HGF in the CNS delays disease progression and prolongs life span in a mouse model of amyotrophic lateral sclerosis (20), a neurodegenerative disease of the nervous system. In addition, HGF is involved in the process of postischemic brain repair (25). Increased concentrations of HGF are detected in the cerebrospinal fluid of patients with inflammatory and demyelinating diseases such as acute demyelinating encephalomyelitis and multiple sclerosis (26).

In addition to its action on the CNS, HGF shows immunomodulatory effects: on the one hand, HGF originally was reported to promote adhesion of B cells (27) and migration of T cells (28) as well as recruitment of dendritic cells (DC) (29). Moreover, HGF was reported to inhibit secretion of TGF-β (30), a potent antiinflammatory cytokine known to inhibit the progression of experimental autoimmune encephalomyelitis (EAE) (31). On the other hand, HGF was identified more recently as having protective effects in animal models of inflammatory-mediated diseases including myocarditis (32, 33), glomerulonephritis (30, 34), inflammatory bowel disease (35), collagen-induced arthritis (36), and pulmonary fibrosis (37).

In the present report, we assess the effect of an overexpression of HGF in the CNS of C57BL/6 mice carrying a HGF transgene under the control of a neuron-specific enolase (NSE) promoter (HGF-Tg mice) leading to selective overexpression of HGF by neurons in the CNS. In contrast, HGF serum levels were similar to those in WT littermate controls. Introduction of HGF under the control of the NSE promoter into mice leads to expression of HGF specifically in postnatal neurons of the CNS and subsequent extracellular secretion of HGF in the CNS, where it can act both on neurons and on other types of postnatal cells, such as glial and immune cells. In this experimental setup, the neural as

Author contributions: M.B., M.-L.S.-R., M.C., and P.H.L. designed research; M.B. and G.S. performed research; H.F. and T.N. contributed new reagents/analytic tools; M.B., M.-L.S.-R., and P.H.L. analyzed data; and P.H.L. wrote the paper.

The authors declare no conflict of interest.

*This Direct Submission article had a prearranged editor.

[1]To whom correspondence should be addressed. E-mail: patrice.lalive@hcuge.ch.

This article contains supporting information online at www.pnas.org/cgi/content/full/0912437107/DCSupplemental.

well as the glial system have been found to be physiologically normal during development and in the adult (20, 38, 39).

EAE induced either by immunization with myelin oligodendrocyte glycoprotein (MOG) peptide consisting of amino acids 35–55 [MOG(35-55)] or by adoptive transfer of T cells from 2D2 transgenic mice that express a T-cell receptor (TCR) specific for MOG(35-55), (TCR^{MOG}) was inhibited before peak disease was reached in HGF-Tg mice. Notably, the level of inflammatory cells infiltrating the CNS decreased in these mice except for $CD25^+Foxp3^+$ regulatory T (T_{reg}) cells, which increased. In addition, a strong T-helper cell type 2 (Th2) cytokine bias was observed: TNF-α, IFN-γ, and IL-12p70 were decreased in the spinal cord of HGF-Tg mice, whereas IL-4 and IL-10 were increased. Antigen-specific response (ASR) assays showed that HGF is a potent immunomodulatory factor that inhibits DC function through down-regulation of their CD40 expression together with a decrease in IL-12p70 secretion. Furthermore, DC treated in vitro with recombinant mouse HGF (rHGF) induced differentiation of IL-10–producing T_{reg} cells, along with a decrease in IL-17–producing T cells and a down-regulation of surface markers of T-cell activation.

Collectively, our data strongly suggest that HGF can inhibit the clinical course of EAE through DC tolerization and induction of T_{reg}-cell population.

Results

MOG-Induced EAE Is Inhibited in HGF-Tg Mice. The HGF content in the spinal cord of HGF-Tg mice, as assessed by real-time PCR and ELISA, was significantly increased (*ca.* 2.5-fold) compared with WT littermates. In contrast, serum levels of HGF, determined by ELISA, did not differ significantly in HGF-Tg and WT littermate mice (Fig. 1*A*) (20). EAE was induced in HGF-Tg and WT littermate C57BL/6 mice using MOG(35-55) peptide. The clinical course of EAE was inhibited in HGF-Tg mice before peak disease was reached [day postimmunization (dpi) 18] until the chronic phase (dpi 45) (Fig. 1*B*). Histopathological analysis of spinal cord performed at peak disease (dpi 25) showed that there was less inflammatory infiltrate (determined by H&E staining) and demyelination (determined by luxol fast blue staining) in HGF-Tg mice, as demonstrated by a decrease in the mean number (± standard error of the mean, SEM) of lesions per slide (Fig. 1 *C* and *D*). Fewer inflammatory $CD4^+$ T-cell, $CD8^+$ T-cell, CD11b, and CD11c cell subtypes were observed in the spinal cord of HGF-Tg mice than in the spinal cord of WT mice (Fig. 1*E*). In addition, Bielschowsky's silver staining indicated a trend toward a decrease in axonal damage in HGF-Tg mice, but the difference did not reach statistical significance (Fig. 1 *C* and *D*).

CNS Overexpression of HGF Does Not Influence Splenocyte Function During EAE. Splenocytes of HGF-Tg mice and WT littermates were isolated at peak disease (dpi 25), and cell surface and intracellular markers were analyzed by flow cytometry. No differences between the two groups of mice were observed in the frequency of $CD4^+$, $CD8^+$, or $CD4^+CD25^+Foxp3^+$ T cells, $CD11c^-CD11b^+$ macrophages, or $CD11c^+$ DC (Fig. 2*A*). When proliferation assays were performed to evaluate the possible influence of CNS-specific overexpression of HGF on peripheral T cells, increased T-cell proliferation was observed with escalating concentrations of MOG peptide, but no difference was observed between HGF-Tg and WT mice (Fig. 2*B*). Analysis of splenocytes by FACS at EAE peak disease was performed with distinction of $CD4^+$ T cells for IFN-γ (T-helper type 1, Th1), IL-10 (Th2), and IL-17 (T-helper type 17, Th17) subsets. No distinction was observed in the spleen for these three $CD4^+$ T-cell subsets when WT and HGF-Tg mice were compared (Fig. 2*C*). To confirm the absence of specific splenic HGF increase in HGF-Tg mice, we analyzed the HGF content from whole spleen in WT and HGF-Tg mice. The results showed no difference in the splenic HGF content in normal and EAE peak-disease conditions (Fig. S1 *A* and *B*). To confirm further that HGF had no effect on splenocyte proliferation during EAE, a proliferation assay with increasing doses of HGF was performed. No proliferation of splenocytes was observed in either WT or HGF-Tg mice at various HGF concentrations (Fig. S1*C*).

Increase of $CD25^+Foxp3^+$ T_{reg} Cells and Induction of a Th2 Cytokine Bias in the Spinal Cord of HGF-Tg Mice During EAE. Inflammatory cell infiltrates from pooled spinal cords of HGF-Tg (n = six mice) and WT littermates (n = five mice) were isolated at peak disease (dpi 25) by Percoll gradient, stained for surface markers, and analyzed by flow cytometry. Compared with WT littermates, a

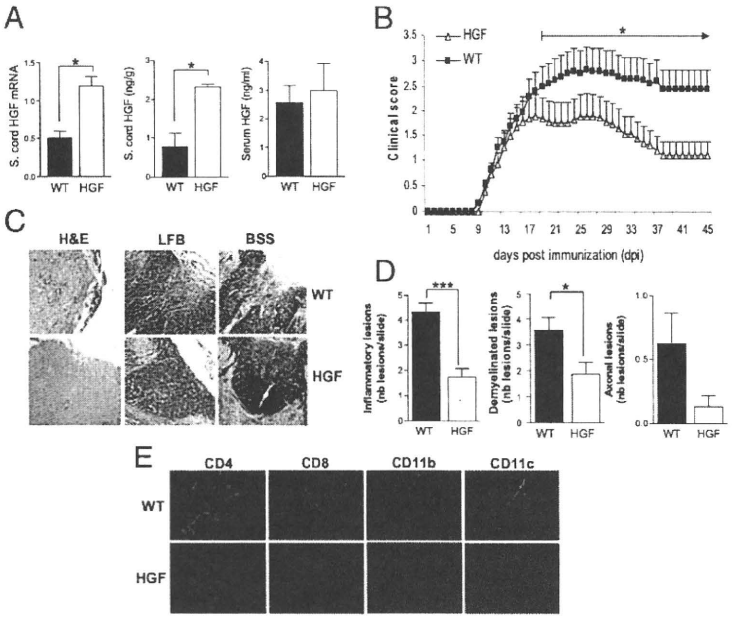

Fig. 1. MOG(35-55)-induced EAE is inhibited in HGF-Tg mice. (*A*) HGF in the spinal cord of HGF-Tg mice versus WT littermates (n = 3 per group) as measured (*Left*) by real-time PCR (relative HGF mRNA expression) or (*Center*) by ELISA (ng/g of spinal cord) (mean ± SEM). *, $P < 0.05$. (*Right*) HGF measured in the serum by ELISA (ng/ml; mean ± SEM). (*B*) EAE scores were determined daily after disease onset in HGF-Tg mice (triangles; n = 17) and WT littermates (squares; n = 18). Shown are mean EAE score ± SEM. The difference was significant before peak disease was reached (dpi 18) and persisted until the chronic phase (dpi 45). *, $P < 0.05$. (*C*) Histopathology of paraffin-embedded spinal cord sections from PBS-perfused WT and HGF-Tg mice at peak disease (dpi 25). Sections were stained with H&E, luxol fast blue (LFB), or Bielschowsky's silver staining (BSS) (magnification 200×). (*D*) Fifteen sections of spinal cord per mouse (n = 6 per group) were analyzed, and the mean number of lesions per slide (±SEM) are presented as histograms. *, $P < 0.05$; ***, $P < 0.001$. (*E*) Representative sections of spinal cord were analyzed. Shown are T-lymphocyte (CD4 and CD8) (red), macrophage (CD11b) (red), and DC (CD11c) (green) infiltration (magnification: 100×).

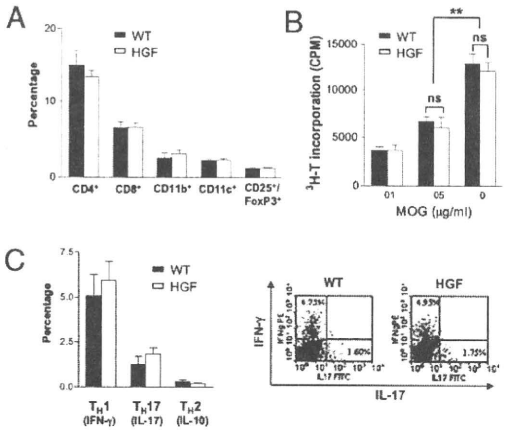

Fig. 2. Unchanged characteristics of splenocyte populations in HGF-Tg mice during EAE. (*A*) Splenocytes were isolated from HGF-Tg mice and WT littermates during EAE and stained for CD4, CD8, CD11b, CD11c, and CD25-FoxP3. Bars show percentages of total splenocytes ± SEM (n = 3 per group). (*B*) Proliferation assay with MOG(35-55) of splenocytes from HGF-Tg mice and WT littermates (mean cpm ± SEM of triplicate experiments; n = 3). **, $P < 0.01$; ns, not significant. (*C*) Analysis by intracellular cytokine staining of the production of IFN-γ (T_H1), IL-10 (T_H2), and IL-17 (T_H17) in splenocytes at peak disease. (*Left*) Bars show percentages of CD4 subtypes ± SEM (n = 6 per group). (*Right*) Representative dot blots of IFN-γ and IL-17 analyses.

decrease of $CD4^+$ and $CD8^+$ T cells, $CD11c^-CD11b^+$ macrophages, and $CD11c^+$ DC was observed in HGF-Tg spinal cords (Fig. 3*A*). In contrast, an increase of $CD25^+Foxp3^+$ T_{reg} cells was observed in the spinal cords of HGF mice (Fig. 3*B*). Intracellular staining for IL-17 production in $CD4^+$ T cells was lower in the spinal cord of HGF-Tg mice than in WT littermates (Fig. 3*C*). In a subsequent experiment, we analyzed by ELISA the cytokines detected in the supernatant of spinal cord homogenate of the two groups of mice. We observed a decrease in TNF-α, IFN-γ, and IL-12p70 in HGF-Tg mice, whereas IL-4 and IL-10 were increased (Fig. 3*D*). The sharp increase in IL-10 (*ca.* 8-fold) was confirmed further by real-time PCR (Fig. 3*E*).

HGF Inhibits Antigen-Presenting Function of DC in Vitro and Induces a Th2 Cytokine Bias. To assess the ability of HGF to influence DC function and T-cell proliferation, we performed a mixed lymphocyte reaction with DC obtained from BALB/c splenocytes and T cells from C57BL/6 spleen cells. In parallel, we confirmed that the cMet receptor was present on the surface of $CD11c^+$ DC of C57BL/6 or BALB/c mice but was not expressed by $CD4^+$ T cells (Fig. S2). After incubation with rHGF at various concentrations, DC were cocultured with T cells, and a proliferation assay was performed using ^{3}H-thymidine incorporation. T-cell proliferation was inhibited in a dose-dependant manner when allogeneic DC were pretreated with rHGF (Fig. S3). We further evaluated the ability of rHGF to inhibit DC function in an in vitro model closer to EAE, i.e., an ASR assay performed with MOG(35-55). In this experiment, DC were purified from C57BL/6 mouse splenocytes and then were treated with rHGF at various concentrations (1–100 ng/mL) or were left untreated and finally were pulsed with MOG(35-55) peptide (20 μg/mL). In parallel, TCR^{MOG} T cells were obtained from splenocytes of 2D2 mice. After 48 h of coculture, T-cell proliferation was measured. A significant inhibition of T-cell proliferation was observed with increasing concentrations of rHGF (10–100 ng/mL), with the maximum effect starting at 30 ng/mL (Fig. 4*A*). To confirm that the inhibition of DC function was indeed mediated through the HGF–cMet pathway, an anti-HGF receptor (α-cMet) neutralizing antibody (10 μg/mL) was added to the DC before incubation with rHGF. Inhibition of T-cell proliferation was abrogated completely by preincubation of DC with the α-cMet antibody across the entire range of tested rHGF concentration (Fig. 4*A*). Furthermore, we examined the expression of T-cell activation markers during ASR assays and found that rHGF-treated DC pulsed with MOG(35-55) were not capable of activating T cells, which remained in a low state of activation ($CD44^{low}CD62L^+$ and $CD44^{intermediate}CD62L^+$). In contrast, when the ASR assays were performed without rHGF pretreatment, T cells were highly activated ($CD44^{high}CD62L^+$ and $CD4^{high}CD62L^-$) (Fig. 4*B*). We then analyzed by ELISA the cytokine secretion profiles in the ASR assay supernatants after DC had been cocultured with TCR^{MOG} T cells. We observed a decrease in TNF-α, IFN-γ, and IL-12p70, whereas IL-4, IL-10 and, to a lesser extent, TGF-β were increased when DC were pretreated with rHGF at 30 ng/mL (Fig. 5*A*). In a subsequent ASR assay, we analyzed intracellular IFN-γ and IL-17 production in $CD4^+$ T cells by flow cytometry and found that IL-17 production was inhibited when $CD4^+$ T cells were cocultured with rHGF-treated DC. In contrast, there was no change in T-cell production of IFN-γ (Fig. 5*B*). Finally, the expression of costimulatory surface molecules on DC (CD40, CD80, CD86, and MHC class II) was measured by flow cytometry during ASR assays. Unlike CD80, CD86, and MHC class II, a decrease in CD40 expression was observed under rHGF influence and was reversed when DC were pretreated with the α-cMet receptor antibody (Fig. S4).

HGF-Treated DC Induce Expansion of $CD25^+Foxp3^+$ T_{reg} Cells in Vitro with Increased IL-10 Production. Because with rHGF pretreatment we observed a strong increase of IL-10 in both the spinal cord of HGF-Tg mice and the DC plus T-cell culture supernatant from ASR assays, we also examined by flow cytometry whether rHGF-treated DC could promote the induction of $CD25^+FoxP3^+$ T_{reg} cells, known to be the major IL-10–producing subtype of T cells. Indeed, a strong increase in $CD25^+FoxP3^+$ T_{reg} cells was observed when rHGF-treated DC, pulsed with MOG(35-55), were

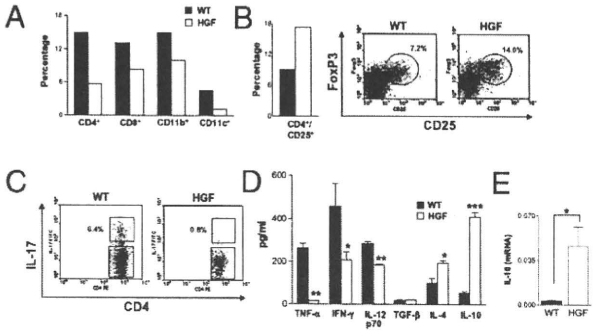

Fig. 3. Spinal cord inflammation of HGF-Tg mice is characterized by a Th2 bias and an increase in T_{reg} cells. (*A*) Inflammatory cells were isolated by Percoll gradient from pooled spinal cords of HGF-Tg (n = 6) versus WT littermates (n = 5) at EAE peak disease (dpi 25) and were stained for CD4, CD8, CD11b, and CD11c. Bars show percentages of total cells. Spinal cord inflammatory cells were stained further (*B*) for CD4-CD25 (histogram; percentage of total $CD4^+$ T cells) and CD4-CD25-FoxP3 (dot blots) or (*C*) for IL-17. (*D*) Spinal cord supernatants from HGF-Tg mice and WT littermates (n = 3 per group) from a subsequent EAE were analyzed by ELISA for cytokines. Shown are the mean ± SEM of experiments performed in triplicate. *, $P < 0.05$; **, $P < 0.01$; ***, $P < 0.001$. (*E*) The increase of IL-10 detected by ELISA in the spinal cord of HGF-Tg mice at peak disease was confirmed by real-time PCR analysis. *, $P < 0.05$.

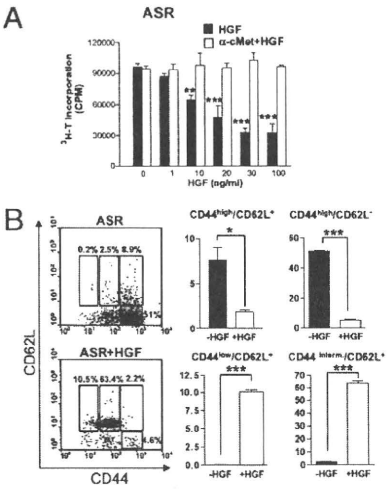

Fig. 4. HGF inhibits in vitro CD11c$^+$ DC function and T-cell activation markers. (*A*) ASR assay performed with C57BL/6 CD11c$^+$ cells stimulated with MOG(35-55) and coincubated with TCR^{MOG} T cells. T-cell proliferation was analyzed after CD11c$^+$ cells were pretreated with α-cMet-blocking antibody or were left untreated and then were preincubated with increasing concentrations of rHGF. **, $P < 0.01$; ***, $P < 0.001$. (*B*) FACS staining for CD44 and CD62L coreceptors of CD4$^+$ T cells after CD11c$^+$ cells were preincubated with rHGF (30 ng/mL) or were not preincubated. Results shown are the mean of three to five independent experiments ± SEM. *, $P < 0.05$; ***, $P < 0.001$.

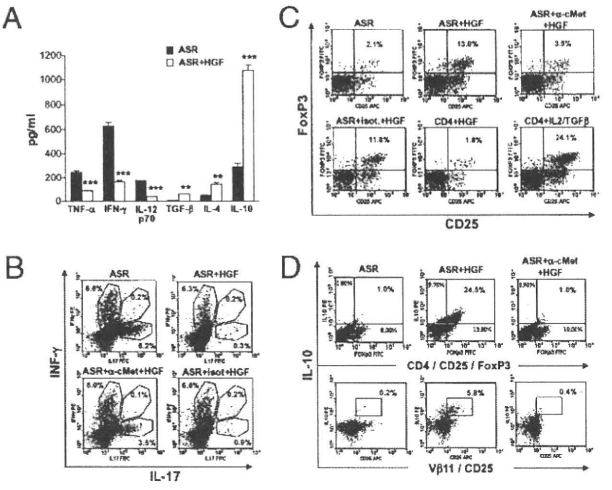

Fig. 5. HGF-treated DC induce a Th2 cytokine bias and CD25$^+$FoxP3$^+$ T$_{reg}$-dependant IL-10 production but decrease IL-17. (*A*) ELISA analysis of cytokines from ASR supernatant: TNF-α, IFN-γ, and IL12p70 are decreased, whereas TGF-β, IL-4, and IL-10 are increased. Results shown are mean ± SEM of triplicate experiments; rHGF added at 30 ng/mL. **, $P < 0.01$; ***, $P < 0.001$. (*B*) Intracellular staining of splenocytes from ASR experiments: CD4$^+$ T-cell–dependant production of IL-17 was inhibited by rHGF-treated CD11c$^+$ cells. Figures are representative of four independent experiments. (*C*) CD4$^+$ T cells were stained for CD25-FoxP3 after CD11c$^+$ cells were treated with rHGF (30 ng/mL) or left untreated. HGF-treated DC induce a strong increase in T$_{reg}$ cells. The effect of HGF on CD11c$^+$ cells was inhibited by preincubation of CD11c$^+$ cells with α-cMet–blocking antibody. HGF had no direct effect on CD4$^+$ T cells, but IL-2/TGFβ–treated CD4$^+$ T cells induced the production of CD25$^+$FoxP3$^+$ T$_{reg}$ cells (positive control). (*D*) IL-10 production (intracellular staining) was increased in CD25$^+$FoxP3$^+$ T$_{reg}$ cells and Vβ11(TCR^{MOG}) CD25 T cells when T cells were cocultured with rHGF-treated CD11c$^+$ cells. This effect was inhibited when CD11c$^+$ cells were preincubated with α-cMet–blocking antibody. Figures are representative of four to six independent ASR experiments.

cocultured with TCR^{MOG} T cells (Fig. 5*C*). This effect was abrogated when DC were pretreated with α-cMet antibody. Also, HGF had no direct influence on CD4$^+$ T cells (in contrast to IL-2 plus TGF-β, which was used as positive control). Intracellular staining performed during ASR assays showed an increase of IL-10 in CD4$^+$, CD4$^+$CD25$^+$ (Fig. S5), and CD4$^+$CD25$^+$Foxp3$^+$ T cells (Fig. 5*D*) when DC were pretreated with rHGF. Again, this effect was reversed by preincubation of DC with α-cMet antibody. In addition, most IL-10$^+$CD25$^+$ T cells were TCR^{MOG} T cells (TCR Vβ11$^+$), demonstrating that MOG autoreactive transgenic T cells could be skewed toward a less inflammatory profile by rHGF-treated DC (Fig. 5*D*).

EAE Induced by Adoptive Transfer of TCR^{MOG} T Cells Is Inhibited in HGF-Tg Mice. To confirm our results further, we performed EAE experiments with adoptive transfer of TCR^{MOG} T cells from 2D2 transgenic mice. EAE was inhibited significantly in HGF-Tg mice, compared with WT littermates, before peak disease was reached (dpi 15) (Fig. 6*A*). At peak disease (dpi 23), analysis of spinal cord-infiltrating inflammatory cells was performed by flow cytometry to evaluate CD25$^+$ IL10-producing T cells as well as surface markers of T-cell activation. The results showed a strong increase in the CD25$^+$IL10$^+$ T-cell population in HGF-Tg mice as compared with WT mice (Fig. 6*B*). Analysis of T-cell activation markers at EAE peak disease confirmed our previous in vitro data (ASR; Fig. 4*B*) by showing that spinal cord CD4$^+$ T cells were maintained in a state of low activation (CD44^{low}CD62L$^+$) in HGF-Tg mice, whereas CD4$^+$ T cells (CD44^{high}CD62L$^-$) were activated mostly in WT mice (Fig. 6*C*).

Discussion

HGF is a pleiotropic factor that acts by binding to the HGF tyrosine kinase receptor, cMet (11). HGF and cMet are expressed in brain-resident cells including neurons (24), mature oligodendrocytes (21, 22), OPC (17, 18, 22), and microglia (19). In addition to its neuroprotective effect, HGF is known to influence inflammation. However, whether its global immunomodulatory effect is pro- or antiinflammatory is still unclear. On the one hand, HGF is known to increase adhesion and migration of inflammatory cells of both the adaptive and the innate immune system (27–29). On the other hand, several antiinflammatory effects of HGF have been described, including (*i*) a Th2/T-helper cell type 3 (Th3) bystander deviation with increase of TGF-β and IL-10 (33, 40), (*ii*) inhibition of antigen-presenting cell (APC) function (40, 41), (*iii*) down-regulation of monocyte chemotactic protein-1 (MCP-1) and regulated upon activation, normal T cell expressed and secreted (RANTES) chemokines (42), and (*iv*) blocking of NF-κB function (42). All these effects could contribute to the protective action of HGF in EAE and/or multiple sclerosis (43, 44).

Here we show that overexpression of HGF in the CNS of transgenic mice inhibits the EAE clinical course by using two different methods of disease induction: MOG immunization and adoptive transfer of MOG-specific T cells. This finding is confirmed by histological observations that show a decrease of inflammatory lesions as well as a lower level of demyelination and axonal loss in HGF-Tg mice. Analyses by flow cytometry of inflammatory cell phenotypes in the spinal cord show that the total number of T cells and APCs was decreased in HGF-Tg mice during EAE, with the exception of the T$_{reg}$ cell population, which increased. Of note, HGF was up-regulated exclusively in the CNS and not in the systemic compartment, as demonstrated by the absence of a significant influence of the transgene on spleen cells. The reduction of CNS inflammation in HGF-Tg mice was associated with a decrease of proinflammatory (Th1) cytokines including TNF-α, INF-γ, and IL12p70, whereas the antiinflammatory (Th2) cytokine IL-10 was strongly increased. In vitro

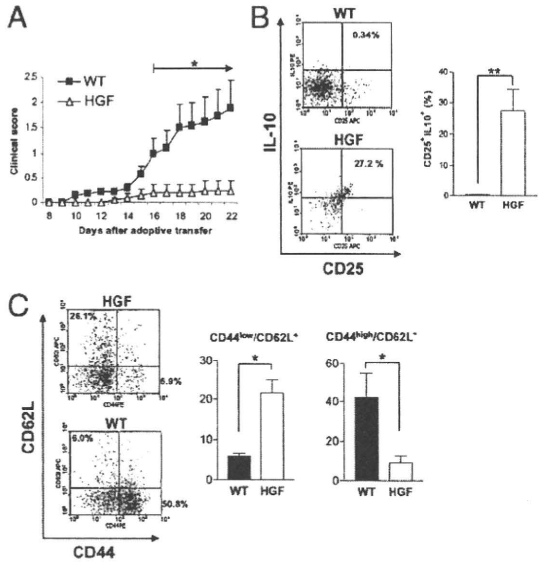

Fig. 6. EAE induced by adoptive transfer of TCR^{MOG}-specific (2D2) T cells is inhibited in HGF-Tg mice. Adoptive transfer of TCR^{MOG} T cells in HGF-Tg mice (n = 10) and WT littermates (n = 12). (*A*) EAE was inhibited in HGF-Tg mice before peak disease was reached. Shown is the mean clinical score ± SEM at day 15 after adoptive transfer. *, $P < 0.05$. (*B* and *C*) Inflammatory cells infiltrating the spinal cord of HGF-Tg mice and WT littermates (n = 5 per group) at EAE peak disease (day 23 after adoptive transfer) were isolated by Percoll gradient and stained by flow cytometry. (*B*) (*Left*) Representative dot blots of CD25 and IL-10 analyses. (*Right*) CD25-dependent IL-10 production was increased in the spinal cord of HGF-Tg mice (mean ± SEM). **, $P < 0.01$. (*C*) Staining for CD44 and CD62L coreceptors showed that $CD4^+$ T cells in the spinal cord of HGF-Tg mice were maintained in a low state of activation. (*Left*) Representative dot blots of CD62L CD44 analyses on T cells. (*Right*) Mean ± SEM, n = 3 per group. *, $P < 0.05$.

assays (i.e., ASR) mimicking immune response during EAE with DC stimulated by MOG with or without HGF and coincubated with TCR^{MOG} T cells demonstrated (*i*) inhibition of DC function (including a decrease in costimulatory CD40 on DC and IL12p70 secretion together with an inhibition of T-cell proliferation), (*ii*) a cytokine Th2 bias similar to that detected in the spinal cord of EAE mice, (*iii*) induction of $Foxp3^+$ T_{reg} cells with a high proportion of IL-10–secreting cells, and (*iv*) inhibition of surface markers of T-cell activation. All these effects were driven by HGF-tolerized DC, and HGF had no direct effect on $CD4^+$ T cells. In addition, the effects of HGF on DC were abrogated when DC were pretreated with blocking antibody directed against cMet, the HGF receptor, thereby indicating that the observed effects were related specifically to DC activation through the HGF–cMet pathway. Finally, EAE experiments were repeated using adoptive transfer of TCR^{MOG} $CD4^+$ T cells, and the results confirmed that inhibition of EAE in HGF-Tg mice is driven specifically through an increase of IL-10–producing T_{reg} cells and maintenance of T cells in a low state of activation.

HGF has been shown previously to be protective in various animal models of immune-mediated diseases such as myocarditis (32, 33), glomerulonephritis (30, 34), inflammatory bowel disease (35), collagen-induced arthritis (36), pulmonary fibrosis (37), allogeneic heart transplantation (45), graft-vs.-host disease (46), and asthma (47). According to these studies, HGF may ameliorate both Th1-type–dominated (33, 36) and Th2-type–dominated (40, 47) autoimmune responses. Interestingly, a recent report demonstrated that, in an experimental model of airway allergy, HGF might repress DC function without up-regulation of IL-10 (40). In contrast, our data along with recent reports on murine models of cardiac transplantation (45) and autoimmune myocarditis (33) clearly show an HGF-dependant induction of both T_{reg} cells and IL-10.

The HGF receptor cMet is not expressed on $CD4^+$ and $CD8^+$ T cells but can be detected on APC including $CD11b^+$ monocyte-macrophages and $CD11c^+$ DC. Of note, DC are the most efficient APC and are crucial in the EAE model, because the presence of DC alone is sufficient to present antigen in vivo to primed myelin-reactive T cells and to mediate CNS inflammation and development of clinical disease (43). Thus, a selective tolerization of DC as demonstrated in the present report could be sufficient to explain the inhibition of EAE. However, because cMet also is expressed on other APC, we cannot exclude completely the possibility that the protective effect of HGF observed in EAE also could be mediated by tolerized monocytes/macrophages.

Two plasminogen-related growth factors have been identified so far: HGF and HGF-like/macrophage-stimulating protein (HGFl/MSP) (48). The receptor for HGFl/MSP is a tyrosine receptor kinase, recepteur d'origine nantais (RON) (49), closely related to cMet, thereby suggesting a coevolution of these growth factors and their receptors. Of note, mice lacking RON show an exacerbation of symptoms during EAE, with overall worsened disease severity, increased demyelination, axonal loss, and neuroinflammation (50). Hence, these data suggest that both HGF and HGFl/MSP are protective in EAE.

In addition to its immunomodulatory effect, the role of HGF in regulating the survival, the differentiation, and the promotion of axonal outgrowth of various neuronal populations, including sensory, sympathetic, and motor neurons, has been firmly established (24). HGF is known to be a potent neuroprotective factor and also is able to induce differentiation of OPC into new myelin-forming cells (18). We recently demonstrated that HGF can be produced by microglia under TGF-β stimulation and can act as a chemotactic factor inducing migration of myelin-forming cells (i.e., OPC) into demyelinated lesions (17). Given that c-Met is expressed and phosphorylated in both OPCs and oligodendrocytes (22) and that activation of caspase-3 in oligodendrocytes can be attenuated by HGF application in the animal model of spinal cord injury (21), we cannot exclude the possibility that the beneficial effects of HGF overexpression in the CNS might be mediated partially via the prevention of oligodendrocytic cell degeneration. The importance of these mechanisms in the attenuation of EAE lesions in HGF-Tg mice remains to be determined.

In conclusion, our data demonstrate that HGF is a strong immunomodulator that inhibits EAE, a model of CNS autoimmunity closely resembling multiple sclerosis. HGF is able to induce tolerization of DC and to inhibit T-cell function at different levels. Our data are in accordance with recent publications showing that the immunomodulatory effects of HGF are mediated through APC tolerization and induction of an antiinflammatory (Th2) cytokine pattern (33, 40, 41). Along with the previous observations that HGF is a strong neuroprotector (24) and potentially could trigger remyelination (17, 18), our results suggest that HGF might be a promising candidate for the development of treatments for immune-mediated demyelinating diseases associated with neurodegeneration, such as multiple sclerosis.

Methods

Mice, Induction of EAE, and Isolation of CNS-Infiltrating Mononuclear Cells. NSE-HGF-Tg mice were generously provided by H. Nakamura and T. Funakoshi (University of Osaka), and genotyping was performed as described (20). The transgenic founder mice (C57BL/6J background) were bred with WT C57BL/6J mice and backcrossed at least 15 times before EAE induction. 2D2 (TCR^{MOG}) transgenic mice were generously provided by V. Kuchroo (Harvard Medical School). All mice were bred in house under pathogen-free conditions and were used at 8–10 weeks of age. Animal experiments were approved by the local veterinary office (Geneva, Switzerland) according to Swiss ethical regulations. For active immunization, female HGF-Tg mice and WT littermates were immunized with MOG(35-55) as described (51). For

adoptive transfer, spleen cells from TCR^{MOG} transgenic mice were stimulated with MOG(35-55) and IL-12p70 (R&D Systems) for 4 days. At day 5, $CD4^+$ T cells were isolated and injected into recipient mice (7×10^6 cells per mouse). Animals received pertussis toxin (300 ng per mouse) on days 0 and 2 after T-cell transfer. Mice were assigned clinical scores daily as described (51). CNS mononuclear cells were isolated as described (52).

ASR Assays and T-Cell Proliferation Assay. $CD4^+$ T cells and $CD11c^+$ cells were selected from spleen cells using MicroBeads (Miltenyi Biotec) according to the manufacturer's protocol. DC were incubated with rHGF (eBioscience) (1–100 ng/mL) for 24 h. As a negative control, DC were preincubated with anti-cMet antibody (10 μg/mL; eBioscience). To examine the effect of HGF on Ag presentation, DC were pulsed with MOG(35-55) (20 μg/mL). After washing with PBS, DC (1×10^5/mL) were cocultured with $CD4^+$ T cells (1×10^6/mL) obtained from 2D2 (TCR^{MOG}) transgenic mice. Proliferation assays were performed as described elsewhere (43).
Methodologies are described in *SI Methods*.

RNA Isolation and Real-Time PCR. RNA was extracted from spinal cords of mice. The spinal cords were flushed with ice-cold PBS, and RNA was isolated using RNAeasy Mini Kits (Qiagen) following the manufacturer's instructions. The PCR was performed as described previously (20). Results were quantified relative to a standard curve generated with serial dilutions of a reference cDNA from a DC line and normalized using TATA-biding protein mRNA. Each experiment was repeated at least three times, and values were expressed as mean ± SEM.

Statistical Analysis. Statistical analysis was performed using two-tailed Student's *t* test. $P < 0.05$ was considered statistically significant.

ACKNOWLEDGMENTS. We thank S. Izui for help in the study design and T. Moll for critically reading the manuscript. We thank C. Juillard, D. Bielser, and G. Brighouse for technical assistance. This study was supported by Grant 310000–113653 from the Swiss National Foundation to P.H.L. and by grants from the Swiss Multiple Sclerosis Society to P.H.L. and from the Alliance SEP Association to P.H.L. and M.C.

1. Birchmeier C, Gherardi E (1998) Developmental roles of HGF/SF and its receptor, the c-Met tyrosine kinase. *Trends Cell Biol* 8:404–410.
2. Nakamura T, Nawa K, Ichihara A (1984) Partial purification and characterization of hepatocyte growth factor from serum of hepatectomized rats. *Biochem Biophys Res Commun* 122:1450–1459.
3. Nakamura T, et al. (1989) Molecular cloning and expression of human hepatocyte growth factor. *Nature* 342:440–443.
4. Stoker M, Gherardi E, Perryman M, Gray J (1987) Scatter factor is a fibroblast-derived modulator of epithelial cell mobility. *Nature* 327:239–242.
5. Gherardi E, Gray J, Stoker M, Perryman M, Furlong R (1989) Purification of scatter factor, a fibroblast-derived basic protein that modulates epithelial interactions and movement. *Proc Natl Acad Sci USA* 86:5844–5848.
6. Weidner KM, et al. (1991) Evidence for the identity of human scatter factor and human hepatocyte growth factor. *Proc Natl Acad Sci USA* 88:7001–7005.
7. Rubin JS, et al. (1989) Purification and characterization of a newly identified growth factor specific for epithelial cells. *Proc Natl Acad Sci USA* 86:802–806.
8. Trusolino L, Comoglio PM (2002) Scatter-factor and semaphorin receptors: Cell signalling for invasive growth. *Nat Rev Cancer* 2:289–300.
9. Matsuda Y, Matsumoto K, Ichida T, Nakamura T (1995) Hepatocyte growth factor suppresses the onset of liver cirrhosis and abrogates lethal hepatic dysfunction in rats. *J Biochem* 118:643–649.
10. Park M, et al. (1986) Mechanism of Met oncogene activation. *Cell* 45:895–904.
11. Bottaro DP, et al. (1991) Identification of the hepatocyte growth factor receptor as the c-Met proto-oncogene product. *Science* 251:802–804.
12. Schmidt C, et al. (1995) Scatter factor/hepatocyte growth factor is essential for liver development. *Nature* 373:699–702.
13. Uehara Y, et al. (1995) Placental defect and embryonic lethality in mice lacking hepatocyte growth factor/scatter factor. *Nature* 373:702–705.
14. Bladt F, Riethmacher D, Isenmann S, Aguzzi A, Birchmeier C (1995) Essential role for the c-Met receptor in the migration of myogenic precursor cells into the limb bud. *Nature* 376:768–771.
15. Honda S, et al. (1995) Localization and functional coupling of HGF and c-Met/HGF receptor in rat brain: Implication as neurotrophic factor. *Brain Res Mol Brain Res* 32: 197–210.
16. Achim CL, et al. (1997) Expression of HGF and cMet in the developing and adult brain. *Brain Res Dev Brain Res* 102:299–303.
17. Lalive PH, et al. (2005) TGF-beta-treated microglia induce oligodendrocyte precursor cell chemotaxis through the HGF-c-Met pathway. *Eur J Immunol* 35:727–737.
18. Yan H, Rivkees SA (2002) Hepatocyte growth factor stimulates the proliferation and migration of oligodendrocyte precursor cells. *J Neurosci Res* 69:597–606.
19. Di Renzo MF, et al. (1993) Selective expression of the Met/HGF receptor in human central nervous system microglia. *Oncogene* 8:219–222.
20. Sun W, Funakoshi H, Nakamura T (2002) Overexpression of HGF retards disease progression and prolongs life span in a transgenic mouse model of ALS. *J Neurosci* 22: 6537–6548.
21. Kitamura K, et al. (2007) Hepatocyte growth factor promotes endogenous repair and functional recovery after spinal cord injury. *J Neurosci Res* 85:2332–2342.
22. Ohya W, Funakoshi H, Kurosawa T, Nakamura T (2007) Hepatocyte growth factor (HGF) promotes oligodendrocyte progenitor cell proliferation and inhibits its differentiation during postnatal development in the rat. *Brain Res* 1147:51–65.
23. Ebens A, et al. (1996) Hepatocyte growth factor/scatter factor is an axonal chemoattractant and a neurotrophic factor for spinal motor neurons. *Neuron* 17:1157–1172.
24. Maina F, Klein R (1999) Hepatocyte growth factor, a versatile signal for developing neurons. *Nat Neurosci* 2:213–217.
25. Miyazawa T, et al. (1998) Protection of hippocampal neurons from ischemia-induced delayed neuronal death by hepatocyte growth factor: A novel neurotrophic factor. *J Cereb Blood Flow Metab* 18:345–348.
26. Tsuboi Y, Kakimoto K, Akatsu H, Daikuhara Y, Yamada T (2002) Hepatocyte growth factor in cerebrospinal fluid in neurologic disease. *Acta Neurol Scand* 106:99–103.
27. van der Voort R, et al. (1997) Paracrine regulation of germinal center B cell adhesion through the c-Met-hepatocyte growth factor/scatter factor pathway. *J Exp Med* 185: 2121–2131.
28. Adams DH, et al. (1994) Hepatocyte growth factor and macrophage inflammatory protein 1 beta: Structurally distinct cytokines that induce rapid cytoskeletal changes and subset-preferential migration in T cells. *Proc Natl Acad Sci USA* 91:7144–7148.
29. Kurz SM, et al. (2002) The impact of c-Met/scatter factor receptor on dendritic cell migration. *Eur J Immunol* 32:1832–1838.
30. Mizuno S, et al. (1998) Hepatocyte growth factor prevents renal fibrosis and dysfunction in a mouse model of chronic renal disease. *J Clin Invest* 101:1827–1834.
31. Kuruvilla AP, et al. (1991) Protective effect of transforming growth factor beta 1 on experimental autoimmune diseases in mice. *Proc Natl Acad Sci USA* 88:2918–2921.
32. Nakamura T, et al. (2000) Myocardial protection from ischemia/reperfusion injury by endogenous and exogenous HGF. *J Clin Invest* 106:1511–1519.
33. Futamatsu H, et al. (2005) Hepatocyte growth factor ameliorates the progression of experimental autoimmune myocarditis: A potential role for induction of T helper 2 cytokines. *Circ Res* 96:823–830.
34. Gong R, Rifai A, Dworkin LD (2006) Anti-inflammatory effect of hepatocyte growth factor in chronic kidney disease: Targeting the inflamed vascular endothelium. *J Am Soc Nephrol* 17:2464–2473.
35. Oh K, et al. (2005) Ameliorating effect of hepatocyte growth factor on inflammatory bowel disease in a murine model. *Am J Physiol Gastrointest Liver Physiol* 288: G729–G735.
36. Okunishi K, et al. (2007) Hepatocyte growth factor significantly suppresses collagen-induced arthritis in mice. *J Immunol* 179:5504–5513.
37. Mizuno S, Matsumoto K, Li MY, Nakamura T (2005) HGF reduces advancing lung fibrosis in mice: A potential role for MMP-dependent myofibroblast apoptosis. *FASEB J* 19:580–582.
38. Kadoyama K, Funakoshi H, Ohya W, Nakamura T (2007) Hepatocyte growth factor (HGF) attenuates gliosis and motoneuronal degeneration in the brainstem motor nuclei of a transgenic mouse model of ALS. *Neurosci Res* 59:446–456.
39. Kadoyama K, et al. (2009) Disease-dependent reciprocal phosphorylation of serine and tyrosine residues of c-Met/HGF receptor contributes disease retardation of a transgenic mouse model of ALS. *Neurosci Res* 65:194–200.
40. Okunishi K, et al. (2005) A novel role of hepatocyte growth factor as an immune regulator through suppressing dendritic cell function. *J Immunol* 175:4745–4753.
41. Rutella S, et al. (2006) Hepatocyte growth factor favors monocyte differentiation into regulatory interleukin (IL)-10++IL-12low/neg accessory cells with dendritic-cell features. *Blood* 108:218–227.
42. Dworkin LD, et al. (2004) Hepatocyte growth factor ameliorates progression of interstitial fibrosis in rats with established renal injury. *Kidney Int* 65:409–419.
43. Greter M, et al. (2005) Dendritic cells permit immune invasion of the CNS in an animal model of multiple sclerosis. *Nat Med* 11:328–334.
44. Sospedra M, Martin R (2005) Immunology of multiple sclerosis. *Annu Rev Immunol* 23: 683–747.
45. Yamaura K, et al. (2004) Suppression of acute and chronic rejection by hepatocyte growth factor in a murine model of cardiac transplantation: Induction of tolerance and prevention of cardiac allograft vasculopathy. *Circulation* 110:1650–1657.
46. Kuroiwa T, et al. (2001) Hepatocyte growth factor ameliorates acute graft-versus-host disease and promotes hematopoietic function. *J Clin Invest* 107:1365–1373.
47. Ito W, et al. (2005) Hepatocyte growth factor attenuates airway hyperresponsiveness, inflammation, and remodeling. *Am J Respir Cell Mol Biol* 32:268–280.
48. Skeel A, et al. (1991) Macrophage stimulating protein: Purification, partial amino acid sequence, and cellular activity. *J Exp Med* 173:1227–1234.
49. Wang MH, et al. (1994) Identification of the ron gene product as the receptor for the human macrophage stimulating protein. *Science* 266:117–119.
50. Tsutsui S, et al. (2005) RON-regulated innate immunity is protective in an animal model of multiple sclerosis. *Ann Neurol* 57:883–895.
51. Burger D, et al. (2009) Glatiramer acetate increases IL-1 receptor antagonist but decreases T cell-induced IL-1beta in human monocytes and multiple sclerosis. *Proc Natl Acad Sci USA* 106:4355–4359.
52. Katz-Levy Y, et al. (2000) Temporal development of autoreactive Th1 responses and endogenous presentation of self myelin epitopes by central nervous system-resident APCs in Theiler's virus-infected mice. *J Immunol* 165:5304–5314.

Journal of Neurochemistry

JOURNAL OF NEUROCHEMISTRY | 2010 | 115 | 1102–1111 doi: 10.1111/j.1471-4159.2010.06979.x

Neuronal over-expression of chromogranin A accelerates disease onset in a mouse model of ALS

Samer Abou Ezzi,* Roxanne Larivière,* Makoto Urushitani† and Jean-Pierre Julien*

*Centre de Recherche du Centre Hospitalier Universitaire de Québec, Laval University, Quebec, Quebec, Canada

†Molecular Neuroscience Research Center, Shiga University of Medical Science, Shiga, Japan

Abstract

Recent studies provided evidence that chromogranins can interact with mutant superoxide dismutase 1 (SOD1) and that chromogranin B (CgB) may act as a susceptibility gene and modifier of onset in amyotrophic lateral sclerosis (ALS). To further investigate the role of chromogranins in ALS pathogenesis, we generated SOD1^{G37R} mice that over-express CgA under the control of Thy1 promoter. Here, we report that neuronal over-expression of CgA in SOD1^{G37R} mice caused acceleration of onset of motor impairment and exacerbation of motor neuron degeneration. The use of monoclonal antibody specific to misfolded mutant SOD1 demonstrated a higher level of misfolded SOD1 species in double transgenic mice compared to SOD1^{G37R} mice, suggesting a stabilization of pathogenic SOD1 species by excess CgA. These results suggest a role of chromogranins as modulators of disease onset in ALS pathogenesis.

Keywords: amyotrophic lateral sclerosis, chromogranins, degeneration, motor neuron, mutant SOD1, transgenic mice.

J. Neurochem. (2010) **115**, 1102–1111.

Amyotrophic lateral sclerosis (ALS) is a progressive adult-onset neurodegenerative disorder characterized by loss of motor neurons in the motor cortex, brainstem and spinal cord. Approximately 10% of ALS cases are familial and 90% are sporadic. For the vast majority of ALS cases, familial and sporadic, the etiology remains unknown. The discovery of missense mutations in the gene coding for the Cu/Zn superoxide dismutase 1 (SOD1) in subsets of familial cases directed most ALS research to elucidating the mechanism of SOD1-mediated disease (Rosen *et al.* 1993). To date, more than 140 different mutations have been discovered in the SOD1 gene that account for ~ 20% of familial ALS cases. These mutations confer a gain of unidentified deleterious properties (Gurney 1994). However, the exact mechanism of disease remains unknown.

Chromogranins are soluble, acidic glycophosphoproteins and are found in large dense core vesicles throughout the endocrine and neuroendocrine system and in neurons from the central and peripheral nervous system (Taupenot *et al.* 2003; Helle 2004; Urushitani *et al.* 2006; Schrott-Fischer *et al.* 2009). Previous evidence suggests an involvement of chromogranins in neurodegenerative diseases (Nishimura *et al.* 1994; Marksteiner *et al.* 2000; Rangon *et al.* 2003). In sporadic ALS patients, the staining pattern of chromogranin A (CgA) is altered in motor neurons and it is co-localized with SOD1 immunopositive aggregates (Schiffer *et al.* 1995; Schrott-Fischer *et al.* 2009). In addition, a CgB gene sequence variation was found to be a risk factor and modulator of disease onset in sporadic and familial ALS (Gros-Louis *et al.* 2009). Recently it has been shown that chromogranin transcripts are dramatically up-regulated when the expression of transactive response DNA-binding protein 43, a protein implicated in transcriptional repression and mRNA processing, is down-regulated (Fiesel *et al.* 2010).

We recently reported that the neurosecretory proteins CgA and CgB can specifically interact with SOD1 mutants to mediate secretion. Moreover, extracellular mutant SOD1 proteins activate microglia and induce motor neuron death in culture (Urushitani *et al.* 2006; Zhao *et al.* 2009). Furthermore, we reported that monomeric SOD1 can be translocated into vesicles of the endoplasmic reticulum-Golgi system and that microsomes are the predominant cellular site

Received July 9, 2010; revised manuscript received August 12, 2010; accepted August 15, 2010.

Address correspondence and reprint requests to Professor Jean-Pierre Julien, Centre de Recherche du Centre Hospitalier de l'Université Laval (CRCHUL), 2705 boulevard Laurier, Québec, QC, Canada G1V 4G2. E-mail: jean-pierre.julien@crchul.ulaval.ca

Abbreviations used: ALS, amyotrophic lateral sclerosis; CgA/B, chromogranin A/B; PBS, phosphate-buffered saline; PFA, paraformaldehyde; SDS, sodium dodecyl sulfate; SOD1, superoxide dismutase 1.

© 2010 The Authors
Journal Compilation © 2010 International Society for Neurochemistry,

of aggregation of mutant SOD1 (Urushitani *et al.* 2008). Taken together, these findings suggest that chromogranin-mediated secretion of mutant SOD1 may contribute to ALS pathogenesis.

To further investigate the *in vivo* implication of chromogranins in ALS caused by mutant SOD1, we generated and analyzed SOD1^{G37R} mice that over-express CgA transgene selectively in neurons (TCgA;SOD1^{G37R}). Here, we report that neuronal over-expression of CgA accelerated disease onset and motor neuron degeneration in SOD1^{G37R} mouse model.

Materials and methods

Antibodies

Antibodies used in immunoblotting, immunohisto- and immunofluorescence include anti-HA (3F10; Roche, Basel, Switzerland), anti-human SOD1 (SOD100; Stressgen, Victoria, BC, Canada), anti-actin (MAB1501; Chemicon, Temecula, CA, USA), anti-Iba1 (Wako, Richmond, VA, USA), anti-Mac-2 (galactose-specific lectin; TIB-166; ATCC, Manassas, VA, USA), anti-glial fibrillary acidic protein (MAB360; Chemicon and Z0334; Dako, Glostrup, Denmark), anti-NFM (clone NN18, Chemicon), SV2 (Developmental Studies Hybridoma Bank, University of Iowa, Iowa, USA) and synaptophysin (Dako) antibodies. We also used mouse monoclonal antibody against mutant SOD1 (clone B8H10), generated in our lab (Gros-Louis *et al.* 2010). B8H10 antibody exhibited selective reactivity for mutant SOD1 species (G93A and G37R) with no reactivity with wild type SOD1, as shown by immunoprecipitation analysis (Fig. 5a).

Animals

Transgenic mice

The DNA construct used to produce mice expressing chromogranin A gene under the control of human Thy1 gene promoter was derived as follows. The human Thy1 vector included the promoter, the first exon, the first intron, and the complete 5′ non-coding region of the second exon of the human Thy1 gene subcloned upstream of a *Hind*III site in the multicloning cassette of pBluescript SK (Beaulieu *et al.* 1999). A 2 kb CgA-HA fragment was obtained by the NgoMIV-EcoRV digestion of a pcDNA3 plasmid containing the full-length murine gene encoding CgA fused to hemaglutinin (HA) coding sequence (Urushitani *et al.* 2006). This fragment was subcloned into the *Hind*III site of the human Thy1 vector. The resulting construct (TCgA) included the human Thy1 gene regulatory sequences followed by the complete coding sequence of mouse CgA gene coupled with HA. TCgA construct was then isolated from vector sequences by digestion with *Pvu*I and *Not*I restriction enzymes. The resulting 5.6 kb linear DNA fragment was microinjected into one-cell mouse embryos of C57BL6/C3H genetic background. The genomic integration of the transgene was confirmed by Southern blot analysis from mouse tail DNA, as described below.

The SOD1^{G37R} (line 29) transgenic mice were a gift from Drs. P. Wong and D. Price from Johns Hopkins University (Baltimore, MD, USA) and have been maintained as C57BL/6 in our laboratory. Double transgenic mice over-expressing CgA and mutant hSOD1^{G37R} (TCgA;SOD1^{G37R}) were derived by breeding mice hemizygous for TCgA and SOD1^{G37R} transgenes.

Analysis of disease onset and survival

Disease course was monitored by a temporal profile of body weight and hindlimb extension reflex once a week using both male and female mice (Urushitani *et al.* 2007). Briefly, mice were suspended by the tail and the extent of hindlimb extension was evaluated as follows: a score of 3 corresponds to normal extension, 2 corresponds to the extension of only one hindlimb and 1 corresponds to absence of hindlimb extension reflex. Disease onset was determined as the time when mice reached their peak body weight before the denervation-induced muscle atrophy and weight loss (Boillee *et al.* 2006; Yamanaka *et al.* 2008; Lobsiger *et al.* 2009). End-stage was defined as the time at which mouse could not right itself within 30 s when placed on its side.

Pre-symptomatic, onset and symptomatic mice refer to 180, 300, and 330 days, respectively. The survival data were analyzed by the Kaplan–Meier life span test and Logrank test ($n = 33$ for TCgA;SOD1^{G37R} mice and $n = 27$ for SOD1^{G37R} mice). The statistical significance of the mean onset of TCgA;SOD1^{G37R} was analyzed by Logrank test. The use and maintenance of the mice described in this article were performed in accordance with the *Guide of Care and Use of Experimental Animals of the Canadian Council on Animal Care.*

Southern blot analysis and PCR

A PCR-amplified fragment of the TCgA construct was used as a 900 bp probe. Genomic DNA extracted from mouse tails was digested with *BamH*I and analyzed according to standard Southern blotting methods (Couse *et al.* 1994). The probe detected a 1.3 kb band in TCgA transgenic mice and no band in wild type mice. TCgA;SOD1^{G37R} mice were then genotyped by two sets of PCR primers for TCgA and SOD1^{G37R} transgenes. The sequences of primers are shown in Table S1.

Immunoblotting and immunoprecipitation of spinal cord tissue lysates

Spinal cord and liver tissues ($n = 3$) were homogenized in TNG-T buffer consisting of 50 mM Tris–HCl (pH 7.4), 150 mM NaCl, 10% Glycerol and 1% Triton-X100 with protease inhibitor cocktail (Roche). Protein concentration was determined by the Bradford method (Bio-Rad, Hercules, CA, USA).

Proteins were denatured by sodium dodecyl sulfate (SDS) sampling buffer containing 10% 2-mercaptoethanol for 5 min at 95°C and were separated by SDS–polyacrylamide gel electrophoresis (PAGE), followed by transfer onto polyvinylidene difluoride membrane (PerkinElmer, Wellesley, MA, USA). Target proteins labelled by primary and peroxidase-conjugated secondary antibody were visualized by chemoluminescent kit (PerkinElmer). For immunoprecipitation study, 300 μg of protein lysates were incubated with 30 μL of Dynabeads® Protein G (Invitrogen, Carlsbad, CA, USA) coupled with mouse monoclonal antibody against mutant SOD1 (Urushitani *et al.* 2007), overnight at 4°C. Immunoprecipitates were eluted in 4% SDS sampling buffer, separated by SDS–polyacrylamide gel electrophoresis and transferred to polyvinylidene difluoride membrane for western blot analysis.

© 2010 The Authors

Tissue collection and *in situ* hybridization

Mice were anesthetized and transcardially perfused with 0.9% NaCl and fixed with 4% paraformaldehyde (PFA) pH 7.4. Spinal cord, brain, gastrocnemius muscles were dissected, post-fixed in 4% PFA pH 7.4 and then placed in phosphate-buffered saline (PBS)-sucrose 20%. Spinal cords were cut on microtome (Leica, Richmond Hill, ON, Canada) in 25 μm sections.

In situ hybridization procedures using S^{35} cRNA probes were performed as described previously (Laflamme *et al.* 1999; Nguyen *et al.* 2001; Urushitani *et al.* 2006), using CgA probes corresponding to the total CgA cDNA. Dark field images of sections of the lumbar spinal cord were used for quantification of CgA over-expression within the gray matter (Figure S1). Images threshold range was set from 1 to 255 and integrated intensity measurement was used to quantify grayscale intensity values of CgA mRNA signal particles using MetaMorph® software (Molecular Devices Inc., Sunny Vale, CA, USA).

Immunohistochemistry and evaluation of gliosis

For immunohistochemistry, spinal cord sections were treated with 0.6% H_2O_2 to inactivate the endogenous peroxidase, and then incubated in the blocking buffer (5% goat serum and 0.25% of Triton-X100 in PBS) before immunoreaction. The primary antibodies used in this study were rat monoclonal anti-HA (1 : 200), mouse monoclonal anti-GFAP (1 : 1000) and rat monoclonal anti-Mac-2 (1 : 500). Immunoreaction with primary antibodies was done overnight at 20°C. Slices were then washed and incubated for 90 min at 20°C with corresponding secondary biotinylated antibody (1 : 750) in blocking solution. After washing, sections were incubated in ABC complex 1 h at 20°C (Vectastain ABC Kit; Vector Laboratories, Burlingame, CA, USA). Staining was developed by incubating the samples in 3′,3′-diamino benzidine tetrachloride solution (substrate kit Vector SG, Vector Laboratories, Burlington, ON, Canada). Tissue samples were counter-stained with hematoxylin (Sigma, St Louis, MO, USA), dehydrated in graded concentration of EtOH and xylene, and coverslipped with DPX (Electron Microscopy Sciences, Fort Washington, PA, USA). The number of Mac-2 positive cells was quantified as described elsewhere (Gowing *et al.* 2008). For GFAP quantification, we performed immunofluorescence on lumbar spinal cord sections from animals at 330 days of age using polyclonal rabbit anti-GFAP (1 : 750) (Dako). The average intensity of GFAP signal was analyzed using MetaMorph® software.

Immunofluorescence and neuromuscular junction staining

Tissue sections were washed in potassium phosphate buffer saline, blocked with 4% goat serum, 0.25% Triton-X100 in potassium phosphate buffer saline and then incubated overnight at 20°C with primary antibody in solution containing 1% goat serum and 0.25% Triton-X100 in potassium phosphate buffer saline. Slices were washed and incubated for 90 min with secondary antibody (Alexa fluor, Invitrogen) diluted 1 : 250. Sections were mounted and coverslipped with Fluoromount G (Cedarlane, Burlington, ON, Canada). For monitoring the neuromuscular junctions, 25 μm gastrocnemius muscle sections were incubated overnight in 0.1 M glycine in PBS at 20°C, and then stained with Alexa Fluor 594-conjugated α-bungarotoxin (1 : 1000, Molecular Probes, Eugene, OR, USA/Invitrogen detection technologies) diluted in 3% bovine serum albumin in PBS overnight at 20°C. After washing in PBS, the muscles were blocked in 3% bovine serum albumin, 10% goat serum and 0.5% Triton-X100 in PBS for 6 h at 20°C. Muscles were then incubated with mouse anti-neurofilament antibody 160 kDa (1 : 2000, clone NN18, Chemicon), mouse synaptic vesicle antibody SV2 (1 : 15, DSHB, University of Iowa, Iowa, USA) and rabbit anti-synaptophysin (1 : 15, Dako) in the same blocking solution overnight at 20°C. After washing in PBS, muscles were incubated with Alexa Fluor® 488 anti-mouse IgG (1 : 500) and Alexa Fluor® 488 anti-rabbit IgG (1 : 250) (Invitrogen), in blocking buffer for 3 h at 20°C. Muscles sections were washed in PBS and finally coverslipped with Fluoromount G (Cedarlane). Total or partial co-localization of α-bungarotoxin with SV2/Synaptophysin/NF-M markers characterizes innervated end-plates and intermediate end-plates, respectively. Whereas, α-bungarotoxin staining alone stands for denervated end-plates. Innervation state was then turned into percentage for statistical analyses.

Morphometric analysis

L5 roots were dissected after perfusion with 4% PFA and then post-fixed in 3% glutaraldehyde. Samples were stained with 2% osmium tetroxide in $NaHPO_4$ 0.1 M for 2 h at 20°C, and then dehydrated in EtOH-acetone. The final dehydration was performed 1 h 20°C with 50% epoxy resin in acetone. Ventral and dorsal roots were properly separated and embedded in epoxy resin at least 2 h 20°C before overnight incubation at 60°C. Resulting blocks were cut in 1 μm semithin sections, stained with toluidine blue and examined by light microscopy. The quantification of L5 ventral root axons was done with the use of MetaMorph® software.

Lumbar spinal cord sections were Nissl stained with thionin. Motor neurons were identified on the basis of their correct location, size (spinal cord ventral horn; laminae IX) and distinct nucleolus. Measurement was performed at the ventral side of a line drawn through the central canal of the anterior horn (Gowing *et al.* 2008).

Sex, group size and statistical tests

Because males and females yielded similar results, the groups consisted of ~ 50% males and ~ 50% females. We used the following group size and statistical tests: for body weight and hindlimb extension reflex ($n = 8$ for each group; unpaired *t*-test), survival ($n = 27$ and 33; Logrank test), end-plate denervation ($n = 4$; two-way ANOVA), motor axon degeneration ($n = 4$; unpaired *t*-test), motor neuron loss ($n = 4$; unpaired *t*-test), immunoprecipitation ($n = 4$; unpaired *t*-test), immunohistochemistry ($n = 4$; unpaired *t*-test).

Results

Generation of transgenic mice with neuronal over-expression of CgA

Transgenic mice with neuron-specific over-expression of CgA (TCgA mice) were generated by microinjecting a Thy1-CgA construct into one cell embryos (Fig. 1a and b). A total of eight founders bearing the Thy1-CgA transgene were obtained. The expression of CgA in the nervous tissues of transgenic mice was investigated by *in situ* hybridization using antisense probe for CgA and by immunohistochemistry

© 2010 The Authors